Spatial relationship between porphyritic Cu-Au mineral occurrences and magnetic signatures within the Iron Mask batholith, south-central Cordillera, British Columbia

M.D. Thomas[1*]

Thomas, M.D., 2021. Spatial relationship between porphyritic Cu-Au mineral occurrences and magnetic signatures within the Iron Mask batholith, south-central Cordillera, British Columbia; in *Targeted Geoscience Initiative 5: contributions to the understanding and exploration of porphyry deposits, (ed.) A. Plouffe and E. Schetselaar; Geological Survey of Canada, Bulletin 616, p. 65–90. https://doi.org/10.4095/327943*

Abstract: Gold-rich porphyry copper deposits are commonly associated with magnetic highs related to high magnetite content—up to 10% volume—within potassium silicate alteration zones. This association promoted magnetic highs as exploration targets. The Iron Mask batholith (comprising Iron Mask and Cherry Creek plutons) contains more than 50 porphyry Cu-Au mineral occurrences, including the New Afton deposit. The batholith's strong positive magnetic signatures permit examining magnetic high correlations with porphyry-type mineralization and evaluating the significance of magnetic signatures for mineral exploration.

Groups of prominent magnetic peaks were delineated, with six and two groups present in the Iron Mask pluton and Cherry Creek pluton, respectively. Mineral occurrences occur within the borders of two groups, but are peripheral to other groups, with the nearest occurrence an average of 500 m from the centre of a group. These close spatial relationships support magnetic exploration for porphyry-copper deposits that significantly narrows the search area. Magnetic exploration is also supported by the observation that porphyry (Cu±Mo±Au) and magnetite-apatite mineralization in the Iron Mask batholith are related to a single intrusive event, a characteristic shared by iron-oxide copper gold deposits, where magnetite-apatite mineralization is located laterally or deeper. The New Afton deposit is situated laterally to the Magnet magnetite-apatite deposit near the end of a linear magnetic high passing through the latter.

Résumé : Les gîtes de cuivre porphyriques riches en or sont généralement associés à des crêtes magnétiques liées à une forte teneur en magnétite — jusqu'à 10 % en volume — dans les zones d'altération à silicates potassiques. Cette association a fait des crêtes magnétiques des cibles d'exploration de choix. Le batholite d'Iron Mask (qui comprend les plutons d'Iron Mask et de Cherry Creek) contient plus de 50 indices de minéralisations porphyriques à Cu-Au, dont le gisement de New Afton. Les fortes signatures magnétiques positives du batholite permettent d'examiner la corrélation entre les crêtes magnétiques et les minéralisations de type porphyrique et d'évaluer l'importance des signatures magnétiques pour l'exploration minérale.

Des groupes de pics magnétiques prononcés ont été délimités, dont six dans le pluton d'Iron Mask et deux dans celui de Cherry Creek. Pour deux d'entre eux, les indices minéralisés se trouvent à l'intérieur des limites du groupe, alors que pour les autres groupes, les indices se situent en périphérie, où l'indice le plus proche se trouve en moyenne à 500 m du centre du groupe. Ces relations spatiales étroites appuient l'utilisation de méthodes magnétiques dans l'exploration des gîtes de cuivre porphyriques en permettant de réduire considérablement l'étendue de la zone de recherche. L'exploration par des méthodes magnétiques est également soutenue par le fait qu'on a constaté que, dans le batholite d'Iron Mask, la minéralisation porphyrique (Cu±Mo±Au) et la minéralisation de magnétite-apatite sont liées à un seul événement intrusif, une caractéristique partagée par les gîtes d'oxydes de fer–cuivre-or, où la minéralisation de magnétite-apatite est située dans une position latérale ou plus en profondeur. Le gisement de New Afton est situé latéralement par rapport au gisement de magnétite-apatite de Magnet, près de l'extrémité d'une crête magnétique linéaire traversant le gisement de Magnet.

[1]Geological Survey of Canada, 601 Booth Street, Ottawa, Ontario K1A 0E8
*Corresponding author: M.D. Thomas (email: mike.thomas@canada.ca)

INTRODUCTION

The Geological Survey of Canada's Targeted Geoscience Initiative program includes the study of several mineral systems, including porphyry-related mineral systems. A particular subproject is investigating Cordilleran Cu±Mo±Au porphyry mineralization in space and time, with one objective being to create an integrated 3-D model of magmatic-hydrothermal evolution within the Triassic alkalic Iron Mask batholith (Fig. 1; British Columbia Geological Survey, 2018a) near the producing New Afton mine (Schetselaar et al., 2017). The batholith hosts numerous mineralized occurrences classified by the British Columbia Geological Survey as showings, prospects, developed prospects, producers, or past producers (British Columbia Geological Survey, 2018b). In addition to hosting porphyry Cu-Au-Ag deposits such as New Afton, Crescent, Pothook, Ajax West, and Ajax East, the batholith contains structurally controlled Cu-magnetite veins (Iron Mask, Makaoo/Python, Grey Mask; Logan and Mihalynuk, 2005) with associated copper mineralization noted in the form of chalcopyrite, malachite, azurite, bornite, and cuprite (British Columbia Geological Survey, 2018c, d). The distribution of these and other occurrences are shown in Figure 2 *after* Logan et al. (2006).

The significant potential for porphyry-type mineralization within the batholith and its association with strong magnetic signatures has prompted a wider examination of the batholith from the perspective of determining the significance of the signatures for mineral exploration. An association of magnetic highs with porphyry deposits had been recognized by Sillitoe (1979), who noted that gold in gold-rich porphyry copper deposits worldwide is normally present in potassium silicate alteration commonly associated with an unusually high magnetite content that could form 3 to 10% of the volume.

The association prompted Sillitoe (1979) to propose that ground or even airborne magnetic surveys could be effective in locating such deposits. If the gold-bearing character of a porphyry prospect could be established, it was suggested that drilling could be focused in the location displaying the highest magnetic response. The observations by Sillitoe (1979) leading to a simplistic correlation between gold-rich porphyry copper deposits and magnetic highs merit attention and make a compelling case for the inclusion of magnetic surveys in exploration for porphyry deposits.

Mineralization and associated alteration and hydrothermal processes can be complex, however, and repeated episodes spanning a protracted period of time can complicate interpretation of the significance of magnetic signatures. Furthermore, spatially and temporally different magmatic events could use the same plumbing/conduit system. Clark (2014) reviewed the magnetic effects of hydrothermal alteration in porphyry copper and iron oxide copper gold (IOCG) systems, noting a requirement to understand the magmatic, metamorphic and hydrothermal processes that create, alter and destroy magnetic minerals to achieve meaningful interpretation of mineralized systems. Arancibia and Clark (1996), in investigating the Island Copper porphyry copper-gold-molybdenum deposit on Vancouver Island, British Columbia, proposed that magnetite-rich vein systems within and around some calc-alkaline porphyry deposits are often pre-mineralization and distinct from magnetite-biotite potassic alteration associated with sulfides and Cu-Au mineralization. The early alteration associated with the Island Copper deposit was generated through moderate to intense Fe metasomatism, whereas the principal Island Copper deposit is associated with a later main-stage phase of potassic alteration that is superimposed on the more extensive early alteration mineralized zone. Gold, although correlating overall with copper and potassic alteration, was probably extensively introduced in the early stage of alteration.

The Island Copper deposit illustrates the kind of complexity that might relate to understanding the significance of a magnetic signature related to a porphyry intrusion. Other complicating factors are rock composition, structure, hydrothermal overprinting, porosity-related fracture systems, oxygen fugacity, and iron and sulfide budgets. Despite the large number of variables, magnetite is commonly a conspicuous mineral within porphyry systems with significant potential to contribute to understanding mineralization-forming processes and exploration; therefore, this paper examines relationships between magnetic signatures, geology, and mineral occurrences within the Iron Mask batholith.

GEOLOGICAL SETTING

The northwest-trending alkalic Iron Mask batholith in the south-central part of the Cordilleran Quesnel terrane (Fig. 1) is a Late Triassic to Early Jurassic magmatic-arc complex (Logan and Mihalynuk, 2005). The batholith includes two principal bodies separated by a broad unit of Eocene alkaline volcanic rocks belonging to the Kamloops Group (British Columbia Geological Survey, 2018a). The latter were inferred to be deposited within a graben structure created by renewed fault movement along the margins of the plutons during Paleocene or Early Eocene time (Kwong, 1987). Logan and Mihalynuk (2005) referred to both the entire alkalic intrusive complex and its larger southeastern portion as the Iron Mask batholith, and the smaller northwestern body as the Cherry Creek pluton. To avoid confusion, the bodies are herein named the Iron Mask and Cherry Creek plutons, respectively (Fig. 1), following usage by Kwong (1987) and more recently in a MINFILE report on the Ajax East past producer (British Columbia Geological Survey, 2018e); Iron Mask batholith will be used when both plutons are the subject of discussion. The batholith is viewed as a subvolcanic, multiple intrusion that is comagmatic and coeval with Upper Triassic volcanic and sedimentary rocks of the Nicola Group, which flank the batholith to the southwest and much of its northeastern margin (Fig. 1; British Columbia Geological Survey, 2018e) and with which the batholith is in intrusive contact (Logan and Mihalynuk, 2005). Middle

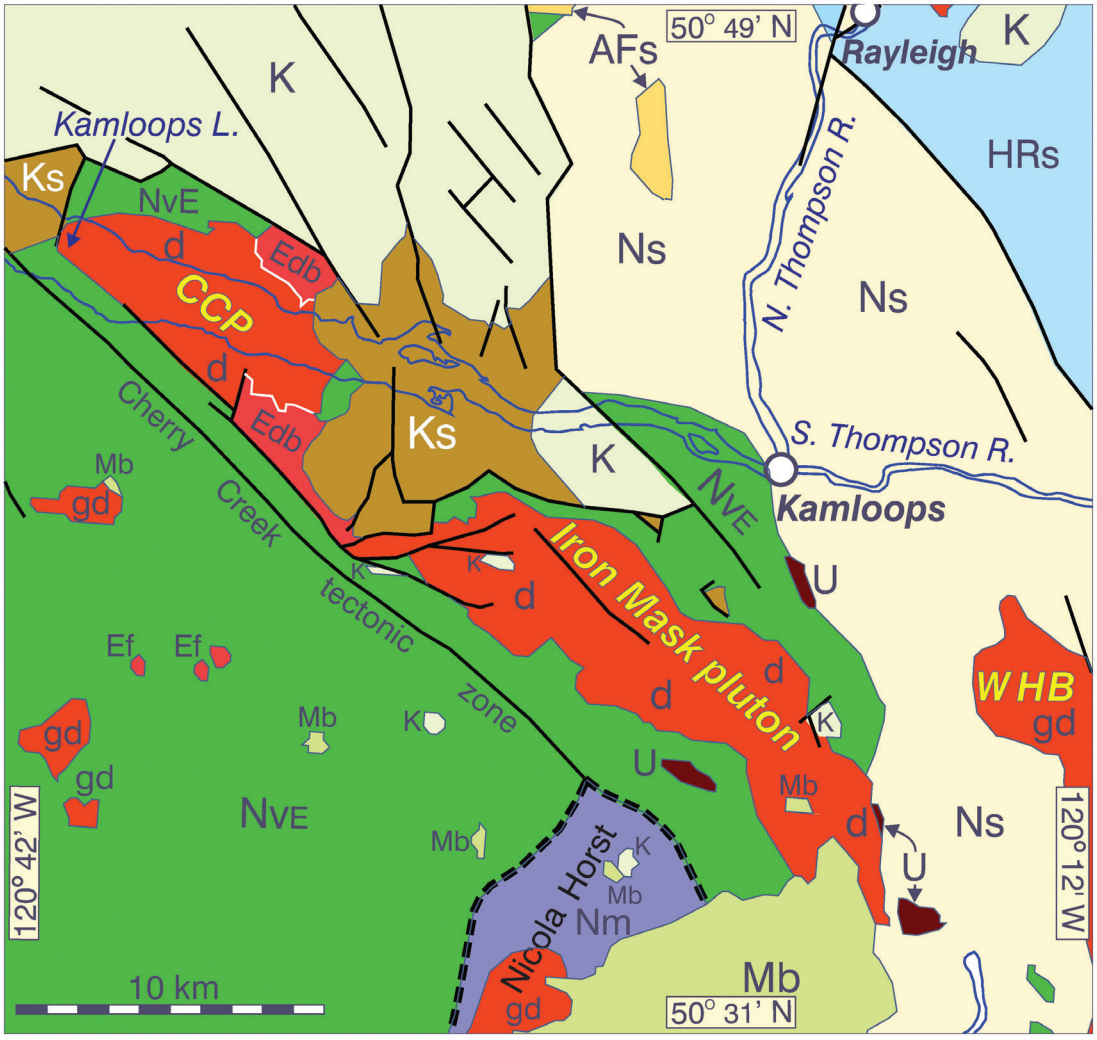

Miocene
- Mb — Basaltic volcanic rocks

Eocene
- K — Kamloops Group, undivided volcanic rocks
- Ks — Kamloops Group, sedimentary rocks

Lower Jurassic–Middle Jurassic
- AFs — Ashcroft Formation, sedimentary rocks

Upper Triassic
- NvE — Nicola Group (Eastern facies), basaltic volc. rocks
- Ns — Nicola Group, fine-grained sedimentary rocks
- Nm — Nicola Group, metamorphic rocks

Devonian–Permian
- HRs — Harper Ranch Group, mudstone, siltstone, shale, fine clastic sedimentary rocks

Intrusive igneous rocks

Eocene
- Ef — Felspar porphyritic intrusive rocks
- Edb — Battle Bluff Complex, diabase, intrusive basaltic rocks

Late Triassic–Early Jurassic
- U — Ultramafic rocks
- d — Dioritic intrusive rocks
- gd — Granodioritic intrusive rocks
- CCP — Cherry Creek pluton
- WHB — Wild Horse batholith
- Fault

Note: Unit abbreviations designated by the author, and are not those used on the MapPlace web site.

Figure 1: Geological map of region including and surrounding Iron Mask batholith that comprises the Iron Mask pluton and Cherry Creek pluton. *Modified from* British Columbia Geological Survey (2018a).

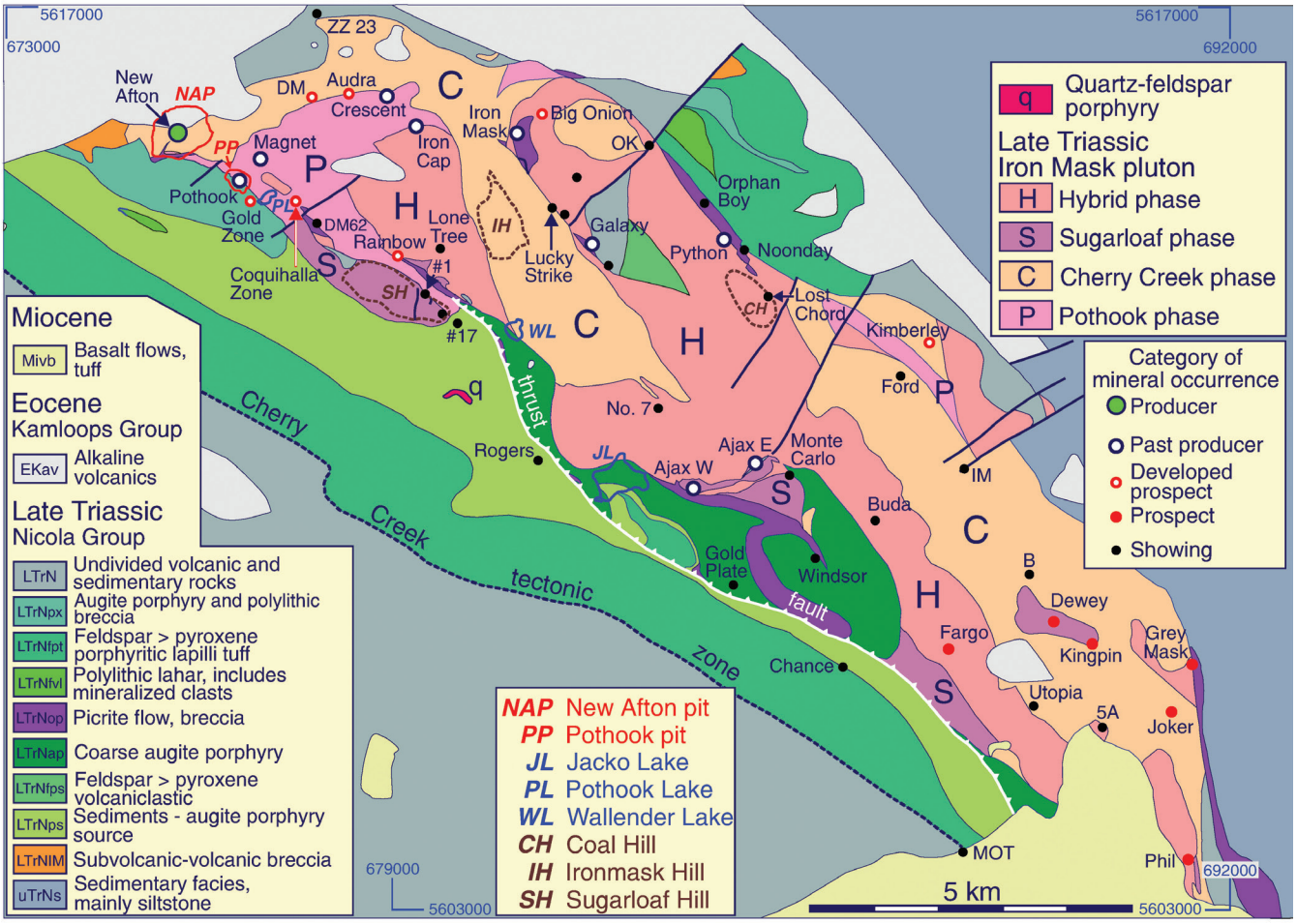

Figure 2: Geological map of Iron Mask pluton *modified from* Logan et al. (2006). Mineralized occurrences as classified by the British Columbia Geological Survey are plotted; some modifications to the category as shown by Logan et al. (2006) are based on more recent information (British Columbia Geological Survey, 2018b). Abbreviations in coloured rectangles of geological legend for Miocene, Eocene, and Late Triassic Nicola Group are those used by Logan et al. (2006). Abbreviations for the phases of the Iron Mask pluton are designated by the author. The age of the quartz-feldspar porphyry unit (q) is not provided.

Eocene volcanic and sedimentary rocks of the Kamloops Group and Miocene alkaline flood basalt unconformably overlie Nicola Group and Iron Mask pluton rocks (Fig. 2). Logan et al. (2006) presented a geological map of the Iron Mask pluton at a scale of 1:25 000 (simplified in Fig. 2) and Logan and Mihalynuk (2005) described the geological units forming the Iron Mask pluton, its porphyry Cu-Au deposits, and marginal Triassic and Eocene units.

Iron Mask pluton

The Iron Mask pluton (Fig. 1, 2) includes three principal intrusions, or phases. In order of decreasing age these are: the Pothook diorite, the Cherry Creek monzonite, and the Sugarloaf diorite (Snyder and Russell, 1993; Logan and Mihalynuk, 2005). A fourth igneous unit, the Iron Mask Hybrid phase, is derived mainly from Pothook diorite and assimilated Nicola Group volcanic rocks. It is a xenolith-rich, heterogeneous unit forming approximately 45% of the batholith. Hybrid rocks mark the contact zones between the three intrusions within the pluton, and between the pluton and volcanic country rock. The xenolith-rich Sugarloaf diorite can also form a hybrid unit. Uranium-lead ages for samples of the Pothook, Hybrid, and Cherry Creek phases are 204 ± 3 Ma, or Upper Triassic (Mortensen et al., 1995). The Sugarloaf diorite is the youngest phase but had not been dated.

Snyder (1994) suggested that magmatic contamination was important in the development of the Iron Mask pluton. The magmatic history is believed to have started with the intrusion of Pothook diorite magma and its interaction with rocks of the Nicola Group that produced the Hybrid unit. Intrusion of the Cherry Creek phase followed closely, possibly partially coeval

with hybridization, and finally Sugarloaf diorite was intruded along pre-existing structures both within the batholith and the Nicola Group country rocks.

The Iron Mask pluton is dominated by the Hybrid and Cherry Creek phases, which cover areas of approximately similar size (Fig. 2). The Hybrid phase is distributed in a Y-shaped belt running parallel to the length of the pluton and occupying much of the southwestern margin and central part of the intrusion. A large belt of Cherry Creek phase flanks the Hybrid phase to the northeast in the southeastern portion of the pluton. A north-northwest-trending unit of Cherry Creek phase lying between the two forks of the Y swings west-southwestward around a belt of Pothook diorite at the top of the western fork and continues to the New Afton pit. A very narrow branch of this Pothook diorite unit extends southeast between the western fork and a short belt of the Sugarloaf phase along the southwestern margin of the pluton. Small units of Pothook, Sugarloaf, and Hybrid phases lie within the unit of Cherry Creek phase in the southeastern part of the pluton. Stanley et al. (1994) reported magnetite concentrations ranging from 10 to 15% in various phases of the pluton. Descriptions of phases of the pluton based on the paper by Logan and Mihalynuk (2005) follow.

Pothook phase

The Pothook diorite is present mainly near the northwestern margin of the pluton, with emplacement apparently controlled by northwest- and northeast-trending faults. The diorite exhibits gradational contacts with the Hybrid unit, faulted contacts masked by strong potassic alteration with the Cherry Creek phase, and reportedly intrusive contacts with the Sugarloaf phase at the Pothook deposit (Stanley, 1994). The Pothook diorite is an equigranular, medium- to coarse-grained diorite containing 40 to 60% plagioclase; 10 to 25% clinopyroxene; 5 to 10% magnetite; 5 to 7% biotite; and up to several per cent K-feldspar, apatite, and lesser accessory minerals. Alteration minerals, including K-feldspar, sericite, epidote, and chlorite, are widespread.

Hybrid phase

The Hybrid phase is a xenolith-rich, heterogeneous igneous component occurring mainly as the extensive Y-shaped belt that traverses most of the Iron Mask pluton. Hybrid rocks delineate contact zones between phases of the pluton, and between the margin of the pluton and volcanic country rocks. Logan and Mihalynuk (2005) noted that Snyder (1994) redefined the Hybrid phase as a facies equivalent of the Pothook diorite, considered to represent outer margins of the Pothook phase that interacted with and incorporated country rock of the Nicola Group. They further noted that the matrix of Hybrid rocks is not necessarily always Pothook diorite, that locally xenolith-rich marginal phases of the Cherry Creek and Sugarloaf phases are hybrid zones and that Snyder and Russell (1995) had subdivided the Hybrid phase into three main types based on texture and clast abundance. From the perspective of studying magnetic signatures of the Iron Mask pluton, the Hybrid phase contains abundant coarse interstitial grains of magnetite in a Pothook dioritic matrix, yielding magnetic susceptibilities typically an order of magnitude higher than most other rock types (Logan and Mihalynuk, 2005). All rock types in the Hybrid unit, which forms approximately 40% of the surface area of the pluton, are described as often containing more than 10% magnetite by volume (British Columbia Geological Survey, 2018f).

Cherry Creek phase

The Cherry Creek phase rivals the Hybrid phase in coverage, forming extensive pluton-parallel belts in both the northwestern and southeastern halves of the pluton (Fig. 2). Historically, there was difficulty distinguishing between Cherry Creek and Pothook phases because of pervasive potassium metasomatism commonly developed adjacent to their contacts (Logan and Mihalynuk, 2005). Textures within the Cherry Creek phase vary from plutonic to hypabyssal and locally volcanic. In the core of the pluton, near Ironmask Hill (Fig. 2), and in the northern part of the southeastern belt, the rocks are leucocratic, fine- to medium-grained, equigranular biotite monzonite. Near the margins of the pluton, rocks are characteristically microporphyries, ranging in composition from monzodiorite to monzonite. Magnetite is disseminated throughout the groundmass in amounts up to 10%.

Sugarloaf phase

The Sugarloaf phase is represented by hornblende porphyritic, trachytic rocks of dioritic composition that crop out mainly along the western margin of the pluton as lenticular bodies or metre-wide dykes in adjacent Nicola Group volcanic rocks. Distribution of the phase was apparently controlled by northwest-trending structures. Dykes of the Sugarloaf phase are oriented radially around Sugarloaf Hill (Fig. 2), interpreted by Snyder and Russell (1993) as a volcanic neck and intrusive centre. The holocrystalline trachytic porphyries of the phase exhibit significant variation in texture, ranging from fine to medium grained. The rocks of the phase are characterized by 1 to 1.5 mm hornblende and plagioclase phenocrysts in a fine-grained groundmass of plagioclase, clinopyroxene, magnetite, and K-feldspar.

Cherry Creek pluton

Kwong (1987) reported that the Cherry Creek pluton consisted entirely of the Cherry Creek unit (i.e. the Cherry Creek phase). As noted in the description of the Iron Mask pluton above, the Cherry Creek phase includes biotite monzonite and microporphyries ranging in composition from monzodiorite to monzonite (Logan and Mihalynuk, 2005).

LARGE-SCALE STRUCTURE OF THE CHERRY CREEK AND IRON MASK PLUTONS

The 3-D geometries of the two component plutons have been investigated by 2-D gravity and magnetic modelling (Thomas, 2019) along lines crossing the central portions of each pluton. Modelling shows the Iron Mask pluton extending from surface to a depth of approximately 5700 m, and laterally for several kilometres on both flanks at a shallow depth below Nicola Group volcanic rocks. The Cherry Creek pluton was determined to be significantly thinner, approximately 2850 m. Magnetic modelling indicates that both plutons are characterized by very steep, relatively narrow magnetic units, and adjacent units may have a significant difference in magnetic susceptibility. The apparent differences in magnetite content are possibly accompanied by petrogenetic differences. Gravity modelling suggests that the densities of diorites in the Cherry Creek pluton are relatively low compared to those in the Iron Mask pluton, hinting that higher density gabbroic varieties may be more prevalent at depth in the latter intrusion.

DISTRIBUTION OF MAGNETIC HIGHS AND PEAK VALUES IN THE IRON MASK AND CHERRY CREEK PLUTONS

The abundance of mineral occurrences (Fig. 2) and strong magnetic signatures within the Iron Mask pluton (Fig. 3), and Sillitoe's (1979) observation of the association of voluminous magnetite with gold-rich porphyry deposits, prompted the examination of magnetic signatures within the pluton from this perspective. Sillitoe (1979) had suggested that if the gold-bearing character of a porphyry prospect could be established, then exploration drilling should be focused in the location displaying the highest magnetic response.

Aeromagnetic coverage of the Iron Mask and Cherry Creek plutons is provided by an airborne magnetic-radiometric survey (Kamloops survey), flown in 2008 over an area centred approximately on Kamloops as a contribution to the Geological Survey of Canada's Mountain Pine Beetle Program (Thomas, 2010). It was flown at 400 m line-spacing and 125 m mean terrain clearance. A higher resolution combined helicopter-borne magnetic-electromagnetic-radiometric survey (Fugro survey) with nominal terrain clearances for the respective instruments of 35 m, 35 m, and 60 m was flown over the northwestern two-thirds of the Iron Mask batholith in 2011 by Fugro Airborne Surveys for New Gold Inc. Flight-lines were oriented northeast and spaced 100 m apart. The potential relationship between magnetic highs and porphyry deposits is examined using magnetic data collected by the higher resolution Fugro survey. These data were kindly made available for analysis by New Gold Inc. with the proviso that magnetic maps produced from the data are not displayed in this report.

Iron Mask pluton

A map of the residual total magnetic field (RTF) over the Iron Mask pluton produced from the Kamloops survey data is presented in Figure 3. The strongest, most positive areas of the magnetic field coincide mainly with most of the Hybrid phase. The magnetic field associated with units of the Pothook and Sugarloaf phases in the northwest of the pluton is also strongly positive, whereas that over the Cherry Creek phase is generally weak throughout the pluton (Fig. 3).

The areas of magnetic highs as displayed in a more detailed image produced from higher resolution Fugro survey data exhibit an apparent roughness, seemingly related to superposed short wavelength magnetic highs. Although the detailed image clearly displays the distribution of the main areas of relatively positive and negative magnetic anomalies, the blending of the various shades of red defining the positive anomalies makes it difficult to clearly identify individual smaller wavelength magnetic highs and the degree to which the magnitude of the field changes over short distances. This problem is alleviated by applying a process to define individual peaks in the grid of values defining the magnetic field. The algorithm compares the value of each grid cell with the values of the surrounding eight grid cells (along the row, column, and both diagonals). A grid cell is defined as a peak when the values of all eight surrounding grid cells are lower. A series of ranges of grid peak sizes is then defined and peaks within these ranges can be colour-coded to help recognize their magnitude. Peak locations and magnitudes are displayed in Figure 4, superposed on the map of the Iron Mask pluton *after* Logan et al. (2006). Concentrations of peaks having noticeably stronger magnitudes have been partitioned into six groups, numbered 1 through 6 (Fig. 5).

Relationship of groups of magnetic peaks to locations of mineral occurrences

A belt of eight strong magnetic peaks (Group 1) runs approximately 1500 m east-southeast from the edge of the producing New Afton pit. Values range from approximately 1625 to 12 240 nT, including four values greater than 3500 nT, with the strongest one positioned on the Magnet past producer. The background level of the magnetic field is locally generally less than 500 nT, dipping down into negative values. The New Afton deposit is hosted in the Cherry Creek phase of the pluton and the Magnet past producer is in the Pothook phase. Curiously, this linear belt of peaks crosses the mutual boundary of the phases at practically right angles, which probably indicates structural control.

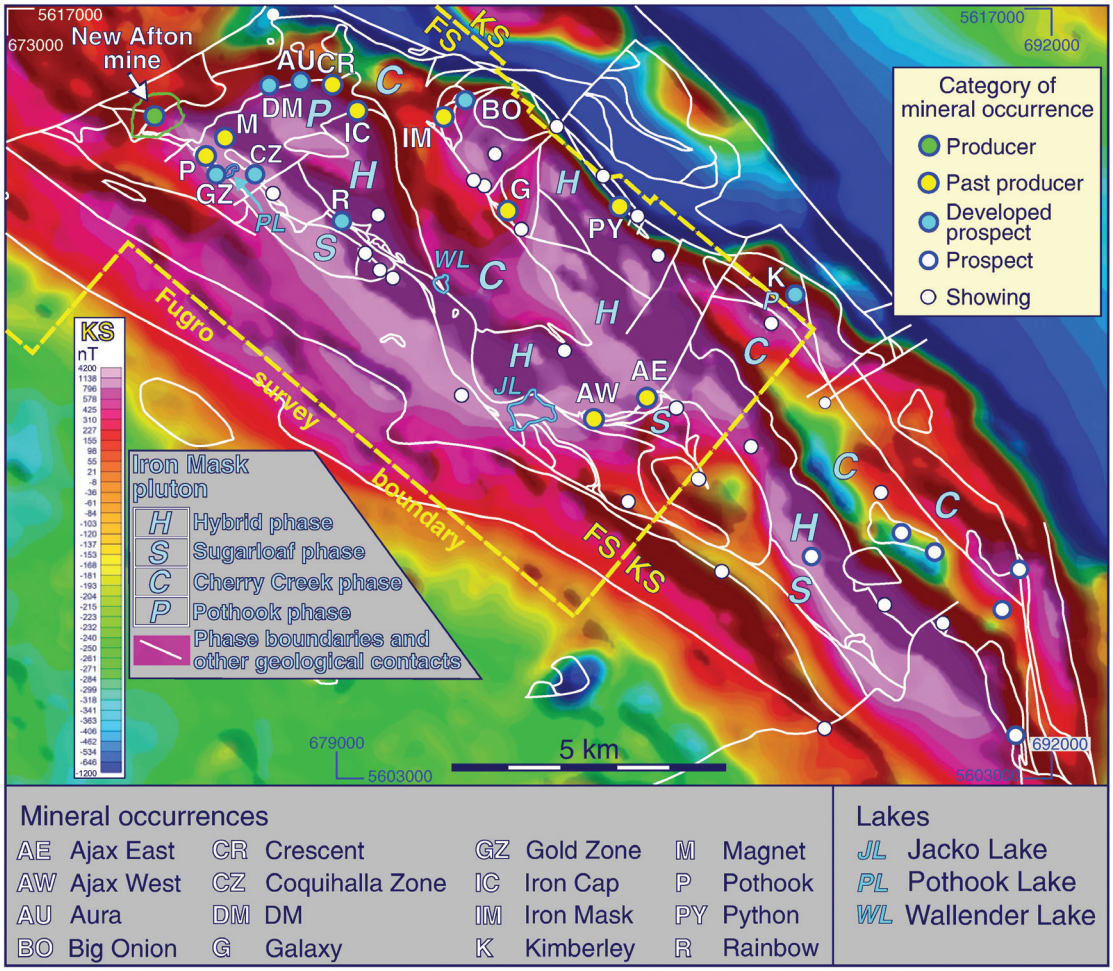

Figure 3: Residual total magnetic field over the Iron Mask pluton defined by the Kamloops survey. The area of higher resolution magnetic data defined by the Fugro survey used to define magnetic peaks is outlined. Geological contacts from a map by Logan et al. (2006) and mineral occurrences (Logan et al., 2006; British Columbia Geological Survey, 2018b) are plotted. FS, Fugro survey; KS, Kamloops survey.

Another conspicuous group of peaks (Group 2), somewhat loosely clustered, is centred approximately 640 m south-southwest of the past-producing Crescent deposit, 650 m west-southwest of the past-producing Iron Cap deposit, and a more distant 1130 m southeast of the DM developed prospect. The Crescent and DM occurrences are hosted by the Pothook and Cherry Creek phases, respectively, and the Iron Cap deposit is located at the boundary between the Cherry Creek and Hybrid phases. The Group 2 peaks range from approximately 2000 to greater than 4900 nT, with most being greater than 3000 nT. Local background values are variable, ranging from approximately 1500 nT to negative values.

Four prominent peaks forming a short curvilinear group (Group 3) trend northwest for approximately 650 m along Coal Hill, passing by the Lost Chord showing just 320 m to the northeast. Peak values range from 2660 to 4525 nT relative to local background levels, which are generally less than 1000 nT but can be up to approximately 1350 nT.

Just north of the Ajax West and Ajax East past producers, a branch of the Hybrid unit extends westward for approximately 2.5 km from the main northwest-trending belt of the unit. Its southern margin lies adjacent to the mineral occurrences and a narrow unit of the Sugarloaf phase. Most peak values within the eastern half of the Hybrid branch are in the range of 2000 to 3000 nT, but lower values between 1000 and 2000 nT dominate the western half with several peaks less than 1000 nT (Fig. 4). In comparison, several peaks in the range of 3000 to 4000 nT are observed in the area marginal to the Ajax West deposit. Near the east end of the Hybrid branch a group of peaks having a similar range extends toward the northwest within the main belt of the Hybrid unit from a point just northeast of Ajax East. The groups near the Ajax East and Ajax West deposits are identified as Group 4 and Group 5, respectively (Fig. 5).

A group of eight relatively high values (Group 6) with limited proximity to mineral occurrences trends northwest from Jacko Lake for approximately 1500 m. It traverses mainly the

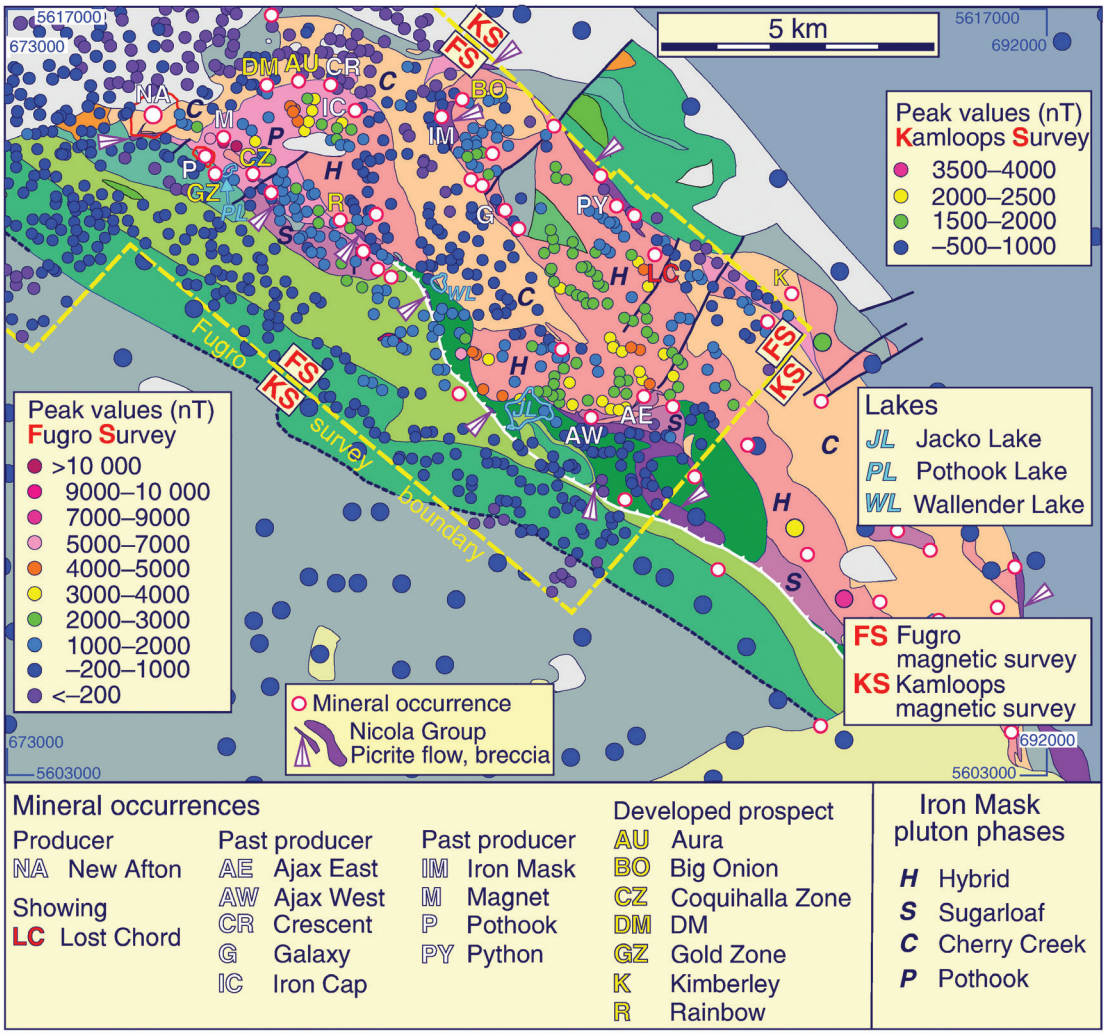

Figure 4: Geological map of the Iron Mask pluton as shown in Figure 2 with locations of mineral occurrences (Logan et al., 2006; British Columbia Geological Survey, 2018b) and magnetic peaks. FS, Fugro survey; KS, Kamloops survey.

Hybrid unit before entering a bordering unit of Nicola Group augite porphyry to the west near its north end. Apart from a relatively weak peak value of 2260 nT at the north end, other values range from 3100 to 5350 nT. With the exception of the highest value, all of the latter peaks (four of which have values greater than 4500 nT) are in the Hybrid unit. The highest peak of 5350 nT is located within the unit of Nicola Group volcanic rocks. The only mineral occurrence close to this group of peaks is the Rogers showing, located 270 m and 210 m southwest of the group and of the boundary between the Hybrid unit and Nicola Group, respectively. The Rogers showing lies within a Nicola Group unit described as sedimentary rocks derived from an augite porphyry source (Logan et al., 2006), though a British Columbia Geological Survey (2018g) MINFILE report identifies the host rocks to be andesitic volcanic rocks. The Rogers showing includes polymetallic veins (Ag-Pb-Zn±Au) and alkalic porphyry Cu-Au mineralization.

Of potential interest for mineral exploration in the area of Group 6 is the presence of a small lens-shaped Nicola Group unit of picrite flow and breccia near the south end of the group at the boundary between the Nicola Group unit hosting the Rogers showing and a Nicola Group unit of augite porphyry (Fig. 2, 4, 5). Such lenses occur intermittently between this occurrence and an occurrence near the New Afton pit and New Afton deposit, forming a discontinuous curvilinear belt falling close to the southwestern margin of the Iron Mask pluton (Fig. 4). Kwong (1987) noted that the picrite unit is one of the geological phenomena associated with hypogene mineralization in the New Afton deposit, further noting that considering wall rocks act as proton sinks during hydrothermal alteration, the presence of picrite is important in the mineralization process, particularly if fractured to enhance the reacting surface area. Kwong (1987)

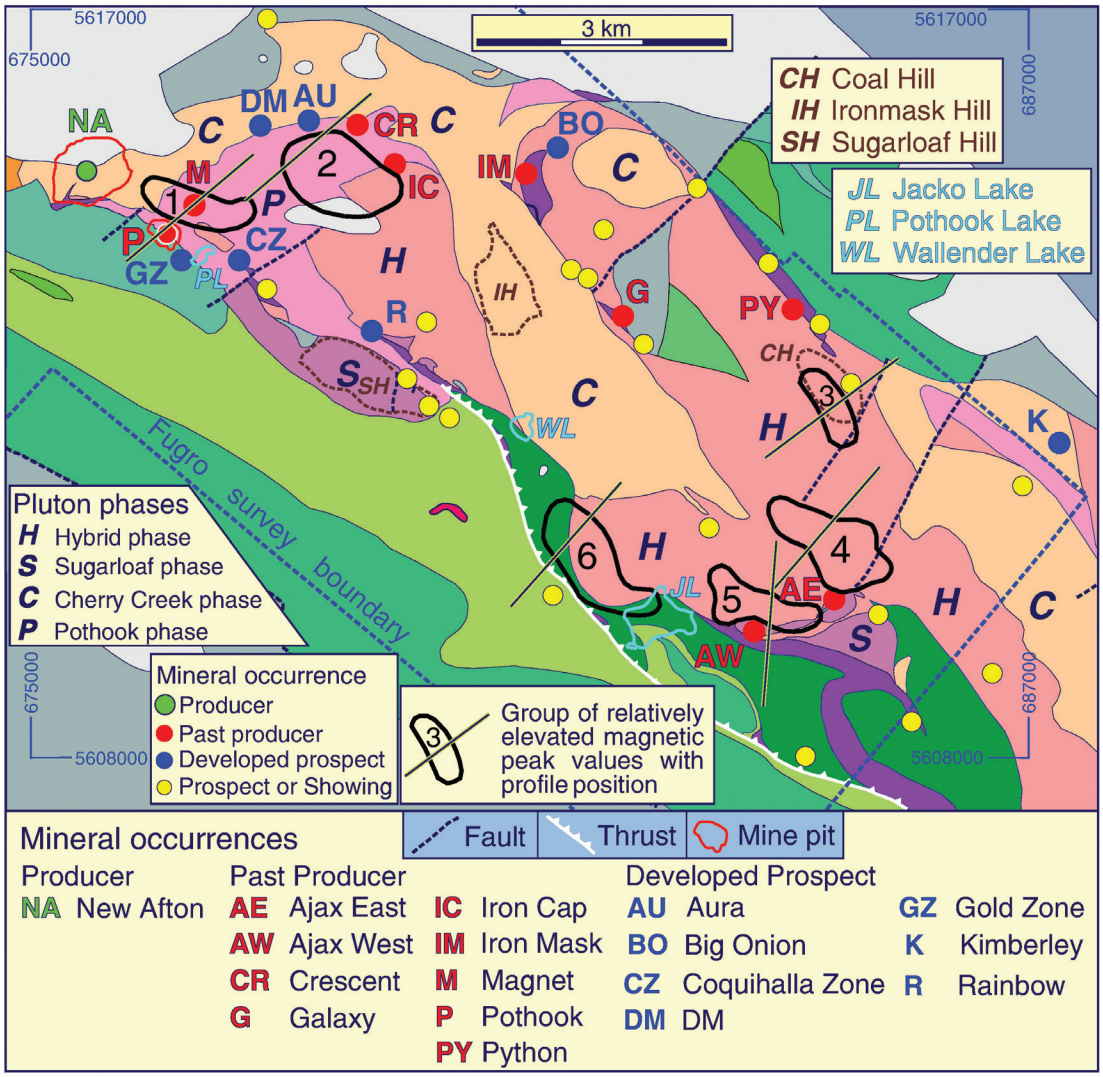

Figure 5: Geological map of the Iron Mask pluton (Logan et al., 2006) displaying locations of mineral occurrences and groups of relatively elevated magnetic peak values. Profile lines for magnetic profiles displayed in Figure 8 are plotted. Complete geological legend is shown in Figure 2.

also drew attention to the fact that picrite bodies, although not well exposed, are generally present within 300 m of most prospects in the district (Carr and Reed, 1976).

Cherry Creek pluton

The Cherry Creek pluton forms the northwest portion of the Iron Mask batholith and is associated with two belts of magnetic highs (Fig. 6): one along its southern margin and the other along the northern margin. Like positive magnetic belts in the Iron Mask pluton, the images of the magnetic field produced from the Fugro survey data exhibit a roughness related to superposed short wavelength magnetic highs. Both plutons are characterized by strong magnetic fields containing magnetic highs having amplitudes greater than 3000 nT. In the Cherry Creek pluton, the eastern part of Kamloops Lake lies between the two belts of magnetic highs, correlating with a relatively smooth magnetic low that is more intense along the southern margin of the lake. In contrast, near the west end of the pluton the lake coincides with part of the northern marginal magnetic high.

Relationship of groups of magnetic peaks to locations of mineral occurrences

Compared to the Iron Mask pluton, the Cherry Creek pluton is relatively poor in mineral occurrences, having just four, although two are past producers. A conspicuous northwest-oriented group (Group 1) of strong magnetic peak values lies between Kamloops Lake and the southwestern margin of the pluton. It extends roughly between

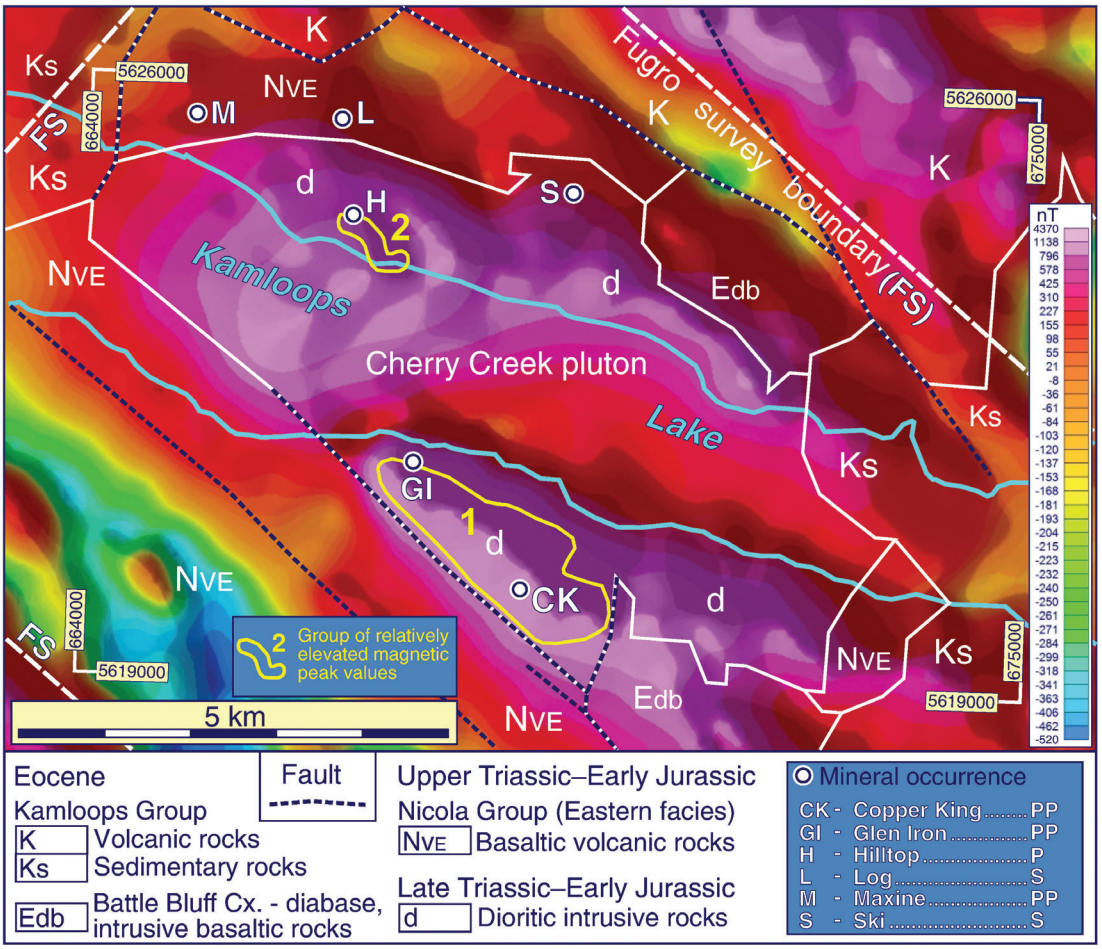

Figure 6: Residual total magnetic field map of Cherry Creek pluton based on the Kamloops aeromagnetic data; the area covered by the Fugro survey is outlined. Geological boundaries and mineral occurrences based on British Columbia Geological Survey (2018a) are plotted. Groups of elevated magnetic peak values (Fig. 7) are outlined. Mineral occurrences are depicted with the same symbol; letters following names indicate the category: PP, Past Producer; P, Prospect; S, Showing.

the past-producing Glen Iron (magnetite, iron) and Copper King (copper, gold, silver, uranium) deposits (Fig. 7). Most peak values fall within the ranges 2000 to 3000 nT or 3000 to 4000 nT and many surround the Copper King deposit. These compare with bordering peak values within the pluton, which are generally in the range of 1000 to 2000 nT or less than 1000 nT, and values within Nicola Group volcanic rocks along the southwest margin of the pluton, which are typically less than 1000 nT. Two small clusters of peaks within Group 1 near the Glen Iron deposit have much stronger values. A cluster southeast of the deposit has values ranging from approximately 5000 to 6250 nT, and the other cluster, immediately southwest of the deposit, has values ranging from 11 000 to approximately 11 680 nT. These very high values close to the Glen Iron deposit are not surprising, given that the deposit comprises magnetite veins varying from less than 30 cm to nearly 10.6 m in width, some of which have been traced for almost 200 m (British Columbia Geological Survey, 2018h). Although magnetite from veins was the main product, Glen Iron is classified as an alkalic porphyry Cu-Au deposit. The Copper King deposit is identified as a polymetallic (Ag-Pb-Zn±Au) vein-hosted deposit within a northwest-trending shear zone (155 × 62 × 55 m) transecting diorite and monzonite of the Cherry Creek pluton and containing chalcopyrite, bornite, pyrite, and magnetite as disseminations and veins (British Columbia Geological Survey, 2018i).

On the north shore of Kamloops Lake, the Hilltop prospect, classified as an alkali porphyry Cu-Au deposit, consists of sparse disseminations of chalcopyrite, bornite, chalcocite, and pyrite in fine- to medium-grained diorites, syenites, and

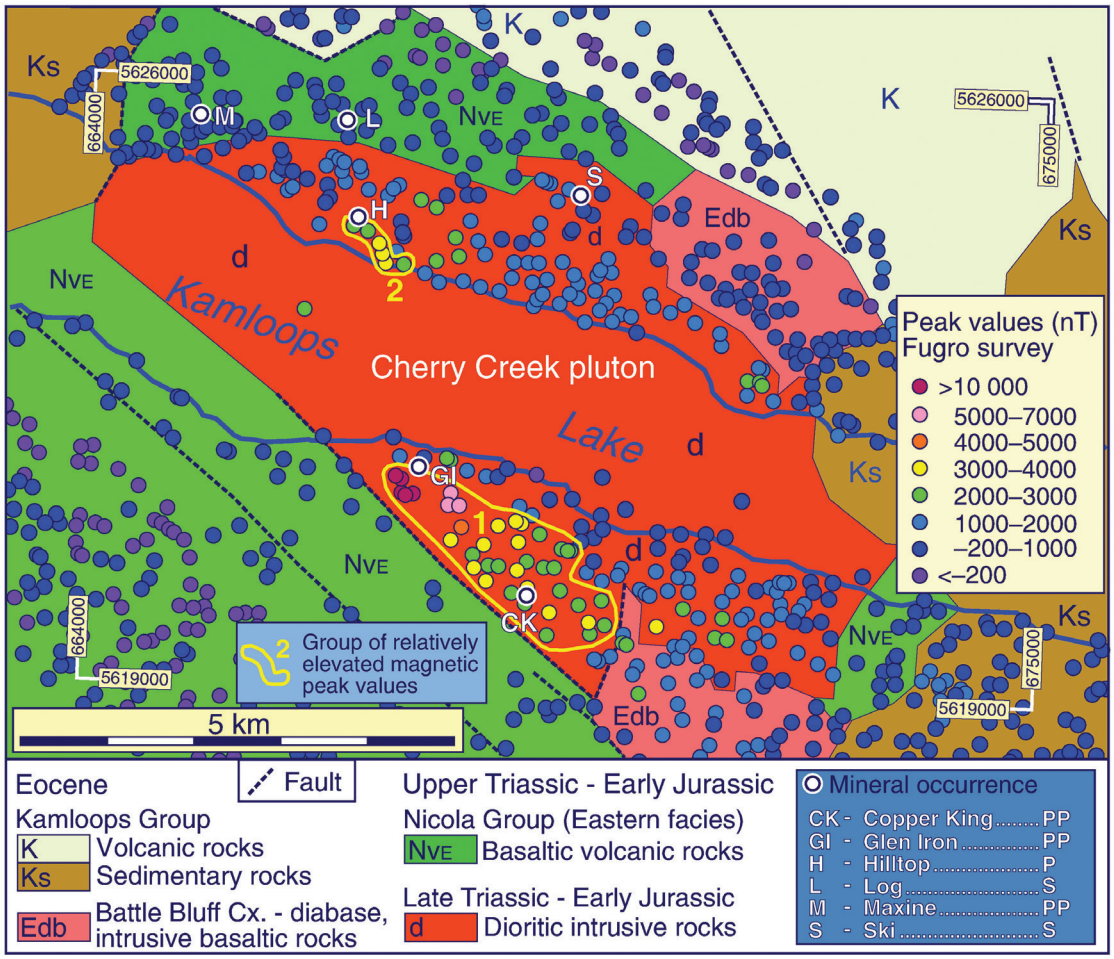

Figure 7: Geological map of the Cherry Creek pluton (British Columbia Geological Survey, 2018a) and magnetic peaks for Fugro magnetic survey data. Mineral occurrences are depicted with the same symbol; letters following names indicate the category: PP, Past Producer; P, Prospect; S, Showing.

monzonites (British Columbia Geological Survey, 2018j). It is located on the northern margin of the only other group of strong peak values (Group 2), which are distributed along a path striking southeast from the deposit (Fig. 7). Three values are greater than 3000 nT and the others are 2320 and 2810 nT; all are significantly larger than proximal peak values, of which roughly half are less than 2000 nT and half are less than 1000 nT. Farther east, the Ski alkalic porphyry Cu-Au showing (British Columbia Geological Survey, 2018k) is not associated with a noticeable magnetic peak. North of the pluton, within marginal volcanic rocks of the Nicola Group, the Maxine past producer (British Columbia Geological Survey, 2018l) and Log showing (British Columbia Geological Survey, 2018m), both classified as alkali porphyry Cu-Au mineralization, occur at or near contacts with rocks of the Cherry Creek pluton. No conspicuous magnetic peaks accompany either mineral occurrence.

SUMMARY OF RELATIONSHIPS BETWEEN MAGNETIC ANOMALIES AND MINERAL OCCURRENCES

The relatively high resolution Fugro survey magnetic data (100 m line-spacing) gridded at a 25 m cell size has defined magnetic signatures at a resolution conducive to relating those signatures to relatively spatially small mineral occurrences within the Iron Mask and Cherry Creek plutons. Both plutons are characterized by strong, expansive positive magnetic signatures, distributed in linear or slightly curvilinear belts running parallel/subparallel to the length of the plutons (Fig. 3, 6).

In the case of the Iron Mask pluton, the generally northwest orientation is doubtless related to its structural setting, which is dominated by north- to northwest-trending high- and moderate-angle faults that likely controlled intrusion of various phases (Logan and Mihalynuk, 2005). Within

the pluton, the signatures are typically associated with the extensive Hybrid phase, though some correlate with smaller areas of the Pothook and Sugar Loaf phases in the northwestern portion of the pluton (Fig. 3). In sharp contrast, the Cherry Creek phase is conspicuous due to its generally muted magnetic signature.

The areas of positive magnetic expression have been examined in detail by defining individual magnetic peaks to estimate the magnitude of shorter wavelength magnetic highs and define their precise locations. This examination enables a greater understanding of the lateral changes in magnetization. Images of the first vertical derivative and tilt angle of the RTF that define short wavelength components of the magnetic field, many having a linear aspect with peaks distributed along them, were also consulted. The spatial relationship of prominent peaks with respect to mineral occurrences has been described, and a close spatial association has been observed in several cases (Fig. 5, 7). Groups of such peaks, indicating relatively high concentrations of magnetite, have been outlined for the Iron Mask pluton (Fig. 5) and the Cherry Creek pluton (Fig. 7).

In the Iron Mask pluton, the locations of Groups 1 and 2 close to many past producers and developed prospects, and to the currently producing New Afton mine (Fig. 5), provide the most persuasive evidence of a genetic connection between the development of magnetite and porphyry-type Cu-Au mineralization. Likewise, the past-producing Ajax East and Ajax West deposits fall on the margins of Groups 4 and 5, respectively. Groups 3 and 6, though they include strong peak values, do not have a close spatial relationship with any mineral occurrences of note. The Lost Chord showing is at the periphery of Group 3, whereas the closest occurrence to Group 6 is the Rogers showing, located 270 m from the group margin within a sedimentary unit of the Nicola Group (Logan et al., 2006) but hosted by andesitic volcanic rocks (British Columbia Geological Survey, 2018g). Despite the lack of mineral occurrences associated with Groups 3 and 6, it is proposed that the areas may hold potential for discovery. The same potential applies to those portions of Groups 2, 4, and 5 that are devoid of occurrences.

In the Cherry Creek pluton, the close relationship between magnetic highs and mineral occurrences is epitomized by Group 1, extending approximately 3 km toward the southeast from the Glen Iron deposit and completely enclosing the Copper King deposit near its southeast end (Fig. 6, 7). Group 2, which is significantly smaller in area, is associated with the Hilltop prospect, one of only two mineral occurrences within the pluton north of Kamloops Lake.

Whereas an unequivocal spatial link between concentrations of magnetite and porphyry-hosted mineral occurrences is apparent, how to best use this relationship to pinpoint the location of mineralization remains a question. The answer is not as simple as Sillitoe (1979) inferred, when he suggested that if the gold-rich character of a porphyry prospect is established, drilling could be focused within portions associated with the strongest magnetic response. Sillitoe noted that high gold values are present mainly in feldspar-stable alteration, commonly of the potassium silicate type. Biotite and K-feldspar (typically in subordinate amounts) are the characteristic alteration minerals. This proposal has merit if the mineralization, alteration, and magnetite-producing phases are co-spatial and coeval. Also, it might require that the various parameters influencing the mineralizing system were essentially uniform throughout, and during the life of the system, which could ensure coproduction of gold and magnetite in much the same relative quantities throughout an eventual deposit. Variation in parameters could possibly result in strong development of magnetite in one part of the system, but weak development of gold. In this situation, using a prominent magnetic signature as a vector for mineralization would be ineffective. As noted by Clark (2014) following a review of magnetic effects of hydrothermal alteration in porphyry copper and IOCG systems, it is necessary to understand the magmatic, metamorphic, and hydrothermal processes that create, alter, and destroy magnetic minerals to achieve meaningful interpretation of mineralized systems.

The fact that porphyry systems may have experienced a series of hydrothermal events is a principal obstacle in evaluating the exploration significance of magnetic signatures. For example, magnetite-rich vein systems associated with some calc-alkaline porphyry deposits may often be pre-mineralization and distinct from magnetite-biotite potassic alteration associated with sulfides and Cu-Au mineralization (Arancibia and Clark, 1996). In their study of the Island Copper porphyry copper-gold-molybdenum deposit, Vancouver Island, moderate to intense Fe metasomatism was believed to have generated early alteration, whereas a later main-stage phase of potassic alteration superimposed on the more extensive early-alteration mineralized zone is associated with the principal Island Copper deposit. Gold, which correlates overall with Cu and potassic alteration, was probably extensively introduced in the early stage of alteration. Arancibia and Clark (1996) also argued that the bulk of magnetite emplacement preceded K metasomatism and the introduction of copper sulfide.

The bulk of copper and molybdenum mineralization in the Island Copper deposit is hosted by flows and pyroclastic rocks of the Bonanza Volcanics and hydrothermal breccias surrounding a major felsic porphyry dyke containing at least 0.1% Cu, but largely sub-ore grade. Despite various episodes of hydrothermal activity, it is perhaps significant that products of the activities exhibit a general spatial coincidence, thus, magnetite as one product of alteration provides a powerful vector toward mineralization via its magnetic signature. Arancibia and Clark (1996) related alteration to a coherent, continuously evolving hydrothermal system associated with subvolcanic intrusive activity centred on the principal porphyry dyke, with superposition of alteration assemblages as a common feature.

The Iron Mask batholith has also experienced several episodes of hydrothermal activity. According to Logan and Mihalynuk (2005), three chemically distinctive hydrothermal events accompanied intrusion and fractionation of its three main phases, the Pothook, Cherry Creek, and Sugarloaf. Copper and gold mineralization are associated with at least two of these phases: the potassic alteration associated with the Cherry Creek monzonite, and the sodic alteration associated with the Sugarloaf diorite. Such alteration may be distributed along extensive belts. The New Afton deposit, for example, lies at the intersection of a corridor of potassic alteration, brittle shearing, hydrothermal breccias, and copper mineralization extending more than 5 km eastward that includes the DM, Audra, Crescent and Big Onion mineral occurrences (Fig. 2), and a corridor of albitic alteration, brittle shearing, and copper-mineralized hydrothermal breccias that includes the Pothook, Rainbow, Ajax West and Ajax East mineral occurrences extending more than 10 km southeastward.

Within these corridors the histories of alteration at several mineral occurrences have been documented in detail. Mineralization is hosted in all phases of the pluton and consists primarily of fracture-controlled chalcopyrite and bornite associated with magnetite, with pyrite, or pyrrhotite occurring peripherally (Logan and Mihalynuk, 2005). Fractures and veins are intimately associated with alteration and mineralization, and various sequences of hydrothermal veins have been documented at different occurrences. At Crescent, within the corridor of potassic alteration, Lang (1994) describes six vein types with crosscutting relationships that allow establishment of a paragenetic sequence. The ore-grade mineralization is associated with chlorite veining. Lang and Stanley (1995) reported that the DM occurrence, within the same corridor, has near-identical characteristics to those of Crescent, with precipitation of copper-gold ore during fracture-controlled potassic alteration, most strongly developed in chlorite-sulfide veins and their alteration envelopes. A series of different vein types is again a characteristic at Pothook, where Stanley (1994) concluded that gold and copper mineralization, hosted in hydrothermal breccia and iron oxide–Cu sulfide (chlorite-epidote) veins, took place after a pervasive albitic alteration, and also at Ajax East and Ajax West deposits (Ross et al., 1995).

SOURCE OF ANOMALIES HAVING ELEVATED PEAKS

Groups of elevated peak values constitute unique signatures within the Iron Mask batholith. Apart from some general correlations with specific lithological units, a link with more specific aspects of the geology is not discerned, with two exceptions: the Magnet past producer (British Columbia Geological Survey, 2018n) in the Iron Mask pluton (Fig. 5), and the Copper King past producer (British Columbia Geological Survey, 2018i) in the Cherry Creek pluton (Fig. 7) are located within the borders of groups. A series of magnetic profiles crossing peak groups in the Iron Mask pluton is displayed in Figure 8. Their paths are plotted in Figure 5. They are derived from the magnetic grid produced from the high-resolution Fugro airborne survey. All profiles are dominated by a central magnetic high, though the high of the profile across Group 6 apparently reflects the coalescence of two separate highs related to two closely adjacent sources. The estimated width at the base of this presumed composite high is much wider (1175 m) than

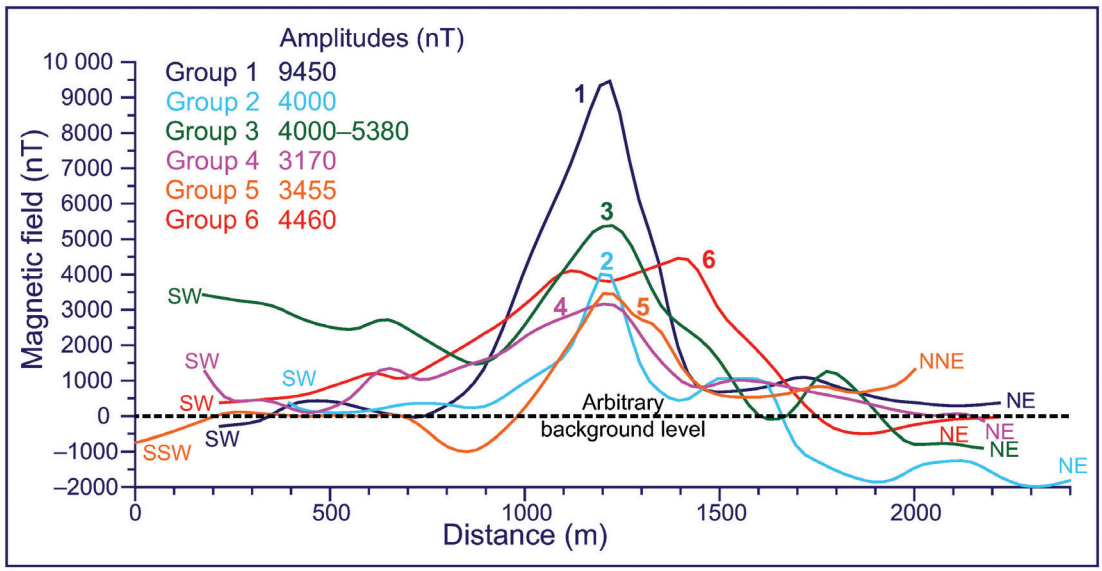

Figure 8: Series of magnetic profiles crossing the various peak groups displayed in Figure 5. Comparison of profiles is enhanced by lining up the central peaks in the profiles. SW, southwest; NE, northeast; SSW, south-southwest; NNE, north-northeast.

those of the other central highs, which are similar and range from approximately 500 to 730 m, even though the range of amplitudes of the central peaks is large: 3170 to 9450 nT.

An opportunity to investigate the potential source of one of these groups is afforded by the presence of the Magnet past producer within the area of Group 1. The investigation is enhanced by access to data collected during a detailed ground magnetic survey (Walcott, 2016, unpub. rept.) that covers most of the area of Group 1.

Model for ground magnetic data within the area of Group 1

A detailed ground magnetic and gravity survey was completed for New Gold Inc. in a small area immediately east-southeast of the New Afton pit, mainly north and northeast of the Pothook pit, with some coverage east and southeast of the Pothook pit (Walcott, 2016, unpub. rept.). The survey covers most of the area of Group 1 peak values (Fig. 5) and is located largely on a unit of Pothook diorite as mapped by New Gold Inc. (Fig. 9a, b). The northeast-trending survey lines have a nominal spacing of between 25 and 50 m, and a total length of approximately 50.5 km. Magnetic readings were taken at 1 s intervals along line, providing a high-resolution grid with a cell size of 5 m.

A total magnetic field image produced from the survey data (Fig. 9a) displays an approximately 1 km long belt of strong positive anomaly trending approximately west-northwest and passing immediately north of the Pothook pit. It trends directly toward the New Afton pit, but terminates within 200 m of the pit at the western limit of the survey. The Fugro and Kamloops survey data indicate this belt continues to just within the easternmost edge of the pit (Fig. 3). Carr and Read (1976) had noted that the Afton deposit (now the New Afton deposit) was located at the west-northwestern end of a conspicuous, 1000 m long, positive aeromagnetic anomaly reflecting a 300 m wide zone of abundant hydrothermal disseminated and vein magnetite, trending northwest from the Magnet deposit to the New Afton orebody. The anomaly terminates in the orebody due to supergene destruction of magnetite.

The belt of strong positive magnetic anomalies, which has a maximum width of approximately 500 m, can be divided into a larger southern element and much smaller northern element near its western end, separated by a narrow, slightly curvilinear magnetic low (Fig. 9a). The low is more pronounced in the east than in the west, where it trends east-west and west-northwest, respectively. Ludwig (2016a, unpub. rept.) proposed that the low might signify the presence of a major structural corridor. The southern magnetic element corresponds with the Group 1 series of peaks defined by the Fugro aeromagnetic survey (Fig. 5), with peaks defined by the ground data displayed in Figure 10a.

The northern element is represented by a single relatively narrow, slightly curvilinear belt of magnetic highs trending west to west-northwest. Its intensity is noticeably lower than the intensities of highs forming a series of narrow, subparallel and intermittently discontinuous linear magnetic highs within the broader southern magnetic element. The trends and definition of all the highs are enhanced in images of the first vertical derivative (Fig. 10b) and tilt (Fig. 10c) of the magnetic field. The highs south of the curvilinear magnetic low generally trend west-northwest in harmony with the trend of the overall composite magnetic high. These highs are transected by faults interpreted from the magnetic data. Some cut across the highs, trending north-northeast to east-northeast, some run subparallel to the essentially west-northwest trend of the highs, and a few trend approximately north-northwest. Faults with various orientations are interpreted north and south of the central belt of positive anomaly.

North and south of the principal belt of magnetic highs the magnetic field is relatively subdued and smooth, though perturbed by some low-amplitude highs. The general background level (areas of green shades, Fig. 9a) is very approximately 56 500 ± 500 nT, with values falling to less than approximately 55 000 nT within some sporadic magnetic lows. In the core area of the positive belt, peak values range generally from 60 000 nT upward; many are between 75 000 and 90 000 nT, with one peak greater than 90 000 nT (Fig. 10a). In terms of amplitude relative to the background field, several peaks have amplitudes of approximately 30 000 nT.

The past-producing Magnet deposit is located on the northern margin of the principal belt of magnetic highs (Fig. 9a) and is the only mineral occurrence associated with the belt. Young and Uglow (1926) described magnetite veins at the Magnet deposit, reporting that the magnetite is generally revealed in shallow trenches and strippings, there being few outcrops. Eight narrow magnetite veins trending mainly east-southeast, an east-trending vein, and an east-northeast-trending vein were interpreted. Widths are variable, ranging from 0.3 to 9.1 m along the length of the veins. Lengths range from a single outcrop a couple of metres long to 427 m. All veins were described to be nearly vertical.

Figure 9: a) Total magnetic field map based on ground survey by New Gold Inc. White circles with black borders indicate mineral occurrences, a legend for which is indicated in b)**.** A-B, line of magnetic model in Figure 11. North-south line labelled 677025 (UTM easting) is line along which inversion of magnetic data was completed by Ludwig (2016b, unpub. rept.). Dashed yellow line labelled F is fault interpreted by Ludwig (2016a, unpub. rept.) to separate a shallow to outcropping magnetite swarm (SOMS) to the west from a buried magnetite swarm (BMS) to the east, linked to the respective magnetic highs in those areas. HMSZ, extent of high magnetic susceptibility (> 300 × 10^{-3} SI) zone at surface defined by Ludwig's (2016b, unpub. rept.) inversion of magnetic data. **b)** Geological map of ground magnetic survey area based on maps by New Gold Inc. and Logan et al. (2006).

a)

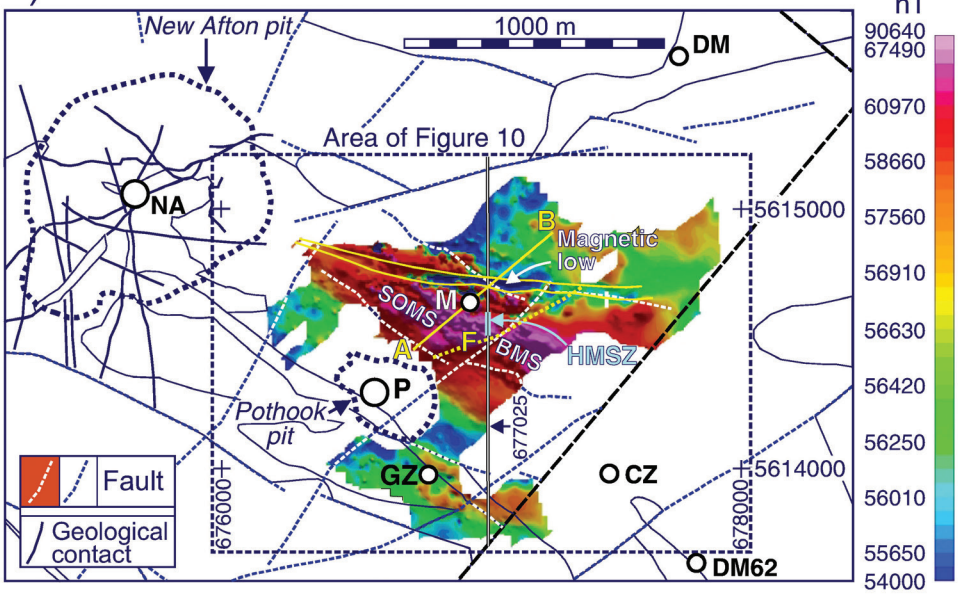

b)

New Gold Inc. legend

Eocene
Kamloops Group
Sedimentary rocks
Jurassic (?)
Conglomerate
Upper Triassic
Nicola Group
Polylithic volcanic breccia
Crystalline volcanic rocks
Picrite
Upper Triassic
Iron Mask pluton
Sugarloaf diorite
Cherry Creek monzonite
Pothook diorite

Logan et al. (2006) legend

Eocene
Kamloops Group
Undivided alkaline rocks
Late Triassic
Nicola Group
Augite porphyry, polylithic breccia
Picrite flow, breccia
Late Triassic
Iron Mask pluton
Hybrid phase
Sugarloaf phase
Cherry Creek phase
Pothook phase

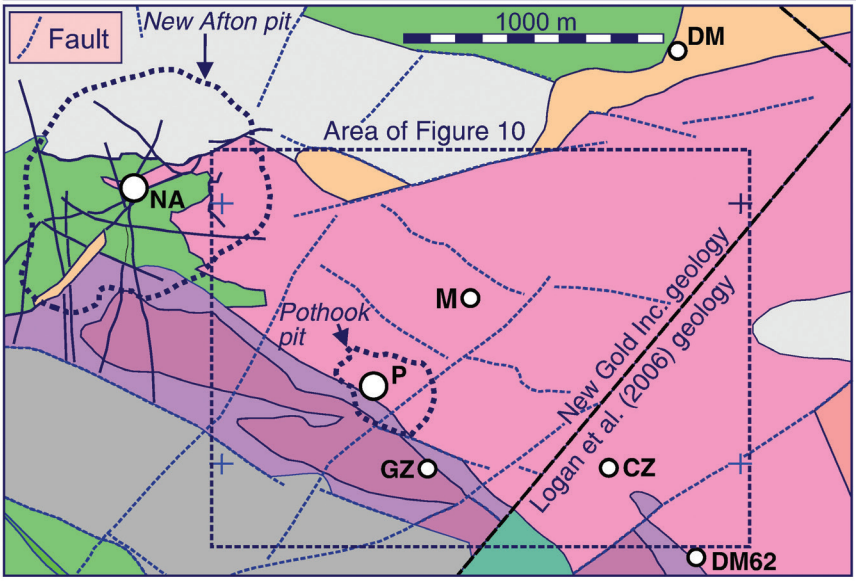

Mineral occurrences

CZ: Coquihalla Zone *(DP)*
GZ: Gold Zone *(DP)*
DM: DM *(DP)*
DM62: DM62 *(S)*
M: Magnet *(PP)*
NA: New Afton *(P)*
P: Pothook *(PP)*

P: Producer
PP: Past producer
DP: Developed prospect
S: Showing

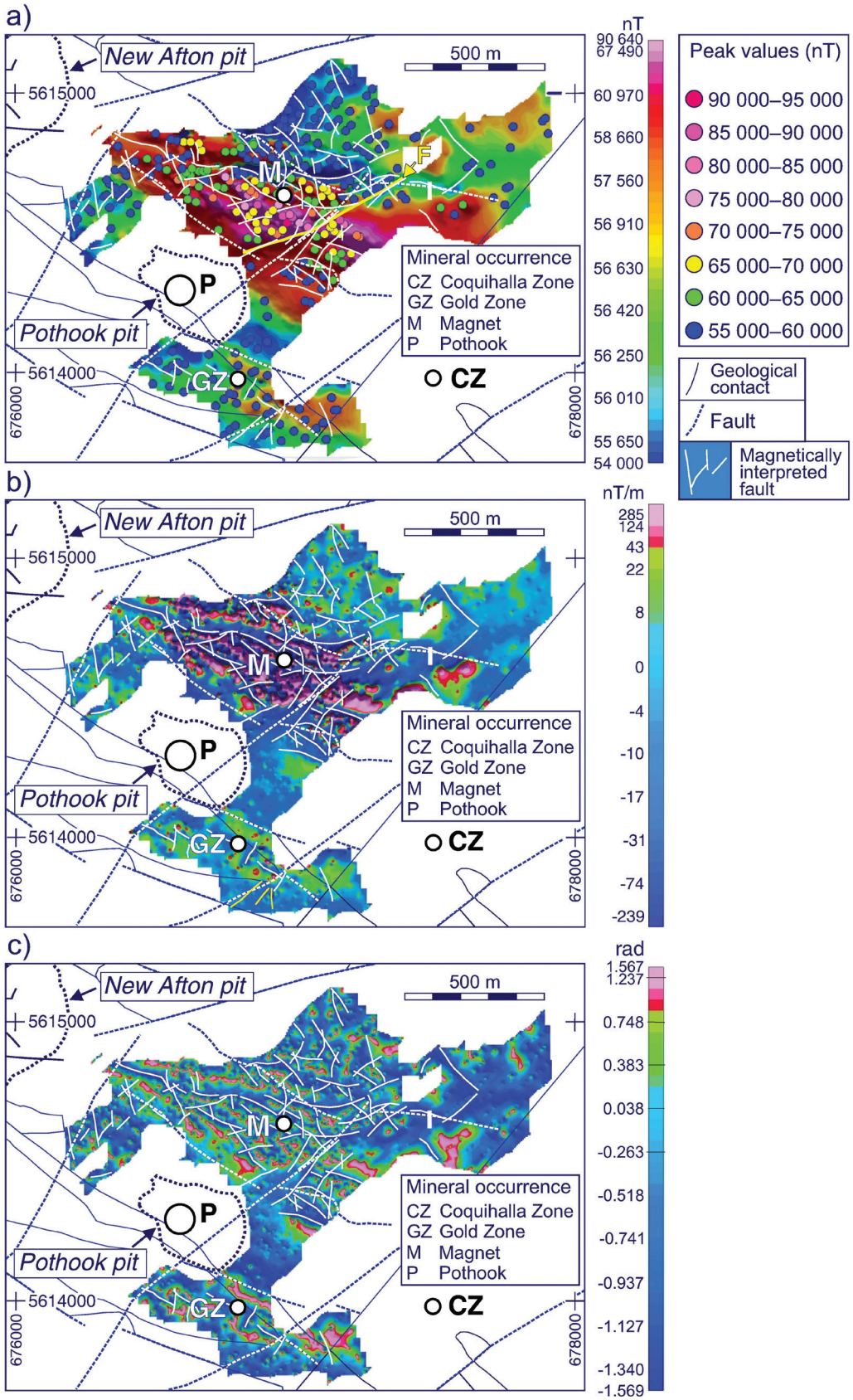

Figure 10: a) Total magnetic field with peak positions for area outlined in Figure 9. F, fault interpreted by Ludwig (2016a, unpub. rept.); **b)** 1st vertical derivative of the total magnetic field; **c)** tilt angle of the total magnetic field.

Young and Uglow (1926) observed that apatite, sometimes in considerable amounts, was commonly associated with the magnetite veins.

Cann (1979) noted that magnetite-apatite lodes (i.e. dykes) in the batholith are tabular bodies up to 200 m long and 6 m wide, containing 50 to 90% magnetite, 10 to 40% apatite, and variable amounts of amphibole. Most are steeply dipping with sharp walls. Their close association with alkaline porphyry-type copper mineralization inspired a proposal that magnetite-apatite lodes could be used as a general exploration guide. Cann (1979) concluded that magnetite-apatite and copper mineralization at the New Afton deposit are genetically linked, but not coeval, because copper mineralization and emplacement of Cherry Creek breccia are younger than magnetite-apatite lodes, with minor younger hypogene copper sulfides present within the lodes. It was believed that the same magma phase was parent to both magnetite and copper mineralization. This conclusion fosters a need to better understand the significance of magnetic signatures, such as those defined by groups of strong magnetic peaks similar to that enclosing the Magnet deposit.

The high-resolution ground magnetic data are used to derive a relatively detailed geological model from the magnetic field. A magnetic profile running southwest-northeast (Fig. 11a) was derived along line A-B passing through the location of the Magnet deposit (Fig. 9a). The geological unit present across the entire profile is the Pothook diorite. Three principal magnetic highs (*a*, *b*, *c*) are present along the southwestern half of the profile, diminishing gradually in amplitude toward the northeast, with the Magnet deposit more or less centred on anomaly *b*. Amplitudes relative to the nadir of the adjacent low to the northeast are 11 600, 10 500, and 6100 nT. The northeastern half of the profile is relatively flat and provides the background level for modelling. In this same area, the Pothook diorite has been assigned a magnetic susceptibility of 20×10^{-3} SI. This value is based on almost 24 000 measurements of drill core samples from the vicinity of the New Afton deposit (mean = 22.6×10^{-3} SI), and 467 measurements of samples of Pothook and Sugarloaf diorites (mean = 19.5×10^{-3} SI). The rounded off value 20×10^{-3} SI represents the non-anomalous background susceptibility.

The magnetic profile is modelled in terms of a series of contiguous, near-vertical, sheet-like units that explain the principal magnetic highs (Fig. 11c). It is assumed that each unit includes magnetite veins similar to those mapped at the Magnet deposit. The different susceptibilities of the sheets, considered as bulk susceptibilities, could thus reflect the variation in size and concentration of veins within the sheets. The sheets range from 12 to 36 m wide and descend essentially from ground surface, at a mean elevation of roughly 740 m above sea level, to a uniform depth of 2000 m below sea level. Upper surfaces of the units actually lie between 5 and 10 m below the ground surface, to simulate the effect of a thin veneer of overburden. The root mean square error (RMSE) of the fit between the observed and modelled profiles is 258.8 nT, which is a good match. A problem with models involving narrow, steep, sheet-like units is that the portions, below a certain critical depth, make a negligible contribution to the magnetic signature of the sheet. Decreasing the depth of the bases of the illustrated sheets from 2000 m below sea level to sea level at intervals of 1000 m produces virtually the same modelled profile, with the RMSE error varying by less than 12 nT (258.8 nT to 246.8 nT). The susceptibility of each sheet remains the same. Raising the bases by another 250 m to lie above sea level does create a noticeable change in RMSE error, which is then 356.5 nT.

It is apparent that a vertical sheet model such as that displayed in Figure 11c, for the indicated susceptibilities, would have a minimum depth to the bottom of the sheets at approximately sea level, roughly equivalent to a depth of approximately 750 m below surface. Ludwig (2016b, unpub. rept.) applied Geosoft's VOXI inversion technique to airborne magnetic data procured for New Gold Inc. in 2005 along lines spaced 100 m apart and oriented north 50° west to south 50° east; flight elevation was quoted to be 'helicopter flying heights'. The data were inverted along UTM easting 677025 passing just east of the Magnet deposit (Fig. 9a) to produce a section of susceptibility values displaying a relatively narrow zone of strong susceptibilities extending from surface to a depth of approximately 1500 m and dipping approximately 75° north. The zone is approximately 250 m wide at surface and increases in width downward to between approximately 700 and 800 m in its lower half, forming an elongate oval that widens toward one end. Characteristic of many inverted models, values increase from the core area outward to the margins, presenting an onion skin pattern. In this model susceptibility values attain a maxima of approximately 630×10^{-3} and 550×10^{-3} SI within the core at depths of approximately 100 and 500 m, respectively.

The model derived from the ground magnetic data (Fig. 11c) presents a similar picture, apart from the distribution pattern of susceptibility values. Instead of the progressive decrease in values outward from the core of the high-susceptibility zone, the ground model has values that constantly vary across the width of the high-susceptibility zone, which has the same 250 m width as the inverted model. Susceptibility values within the individual near-vertical sheets range from 50×10^{-3} to 680×10^{-3} SI, though most values are greater than 210×10^{-3} SI. The 680×10^{-3} SI value is for a near-vertical sheet located within the span of the largest of the three prominent magnetic highs (*a*). Other high susceptibility values for sheets associated with the magnetic highs are 610×10^{-3}, 500×10^{-3}, 385×10^{-3}, and 370×10^{-3} SI, which are consistent with susceptibilities in the inverted model (Ludwig, 2016b, unpub. rept.). The Magnet deposit is located at the southern edge of a 35 m wide sheet with a susceptibility of 610×10^{-3} SI (magnetite content = 19.4%) that is mainly responsible for producing the magnetic high *b* (Fig. 11a). The magnetite dykes defining the deposit (maximum width 9.1 m; Young and Uglow, 1926), do not produce visible individual signatures in this ground magnetic survey, presumably because of their narrow widths.

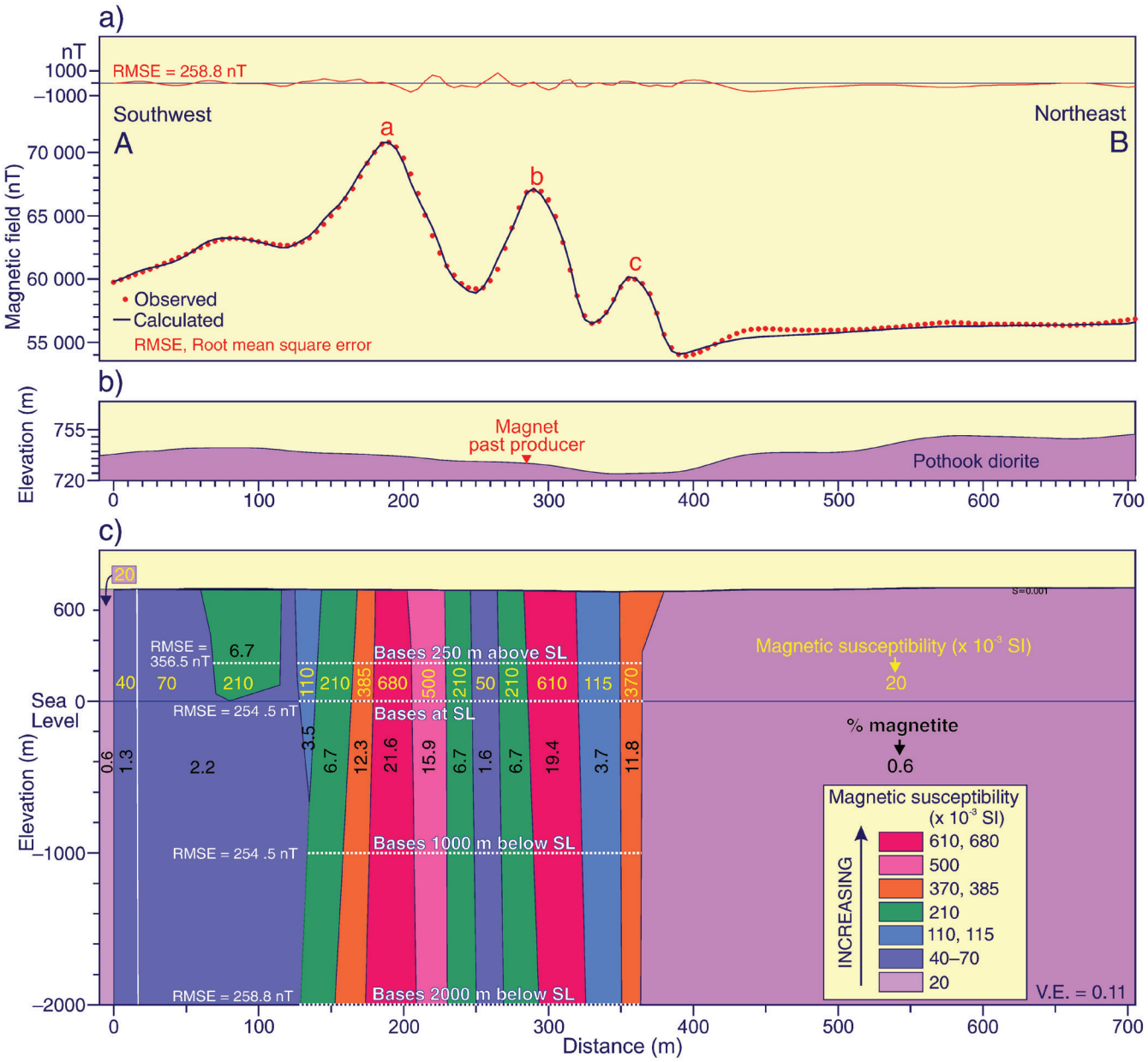

Figure 11: a) Modelled magnetic profile along Line A-B of Figure 9a. **b)** Near-surface geological section. **c)** Magnetic model; the root mean square error (RMSE) for different depths to the bottoms of modelled units is indicated, along with the corresponding positions of the bottoms. V.E., vertical exaggeration.

Transformation of Ludwig's (2016b, unpub. rept.) susceptibility model into percentages of magnetite produces values of approximately 20 and 17% magnetite within the two zones corresponding to the susceptibility maxima, with values decreasing gradually toward the margins of the high-susceptibility zone. Magnetite percentages for the current model were calculated using a formula originally derived by Balsley and Buddington (1958) and modified by McCafferty et al. (2004). Model units co-located with the three prominent magnetic peaks (*a*, *b*, *c*; Fig. 11) have magnetite percentages ranging from 11.8 to 21.6%, and include values similar to those of Ludwig's (2016b, unpub. rept.) model. The current sheet-like model has a different geological significance from that of Ludwig's (2016b, unpub. rept.) onion skin model, that essentially represents a single body within which the susceptibility decreases from the core to the margins. The current model predicts separate contiguous sheets, each of which is believed to include distributed individual magnetite veins. The susceptibility of a sheet represents the weighted mean susceptibility of susceptibilities of veins and relatively non-magnetic host rock. In an earlier qualitative interpretation of the ground magnetic data, Ludwig (2016a, unpub. rept.) defined a northeast-trending fault seemingly sinistrally offsetting the broad

southern portion of the principal belt of magnetic highs (Fig. 9a). West of the fault, Ludwig (2016a, unpub. rept.) noted that linear trends of magnetic highs produced a well-defined, west-northwest-trending grain, attributed to a shallow to outcropping magnetite 'swarm' (SOMS; Fig. 9a). This description is compatible with the near-vertical, sheet-like units of the model in Figure 11c. East of the fault, there are fewer magnetic highs across the width of the belt, though some are very strong, and the magnetic field was related to a buried magnetite swarm (BMS, Fig. 9a). Values of magnetic peaks differ little from west to east across the fault (Fig. 10a), suggesting that magnetite burial on the eastern side of the fault may also be reasonably shallow.

The magnetic model for the Group 1 peaks considered in the context of an essentially co-spatial magnetite vein system provides a geologically reasonable explanation for the magnetic highs within Group 1. It is proposed that the similarity in width of the principal magnetic high in the airborne profile across Group 1 to highs in profiles across other groups (Fig. 8) provides a rationale for considering veins and/or thin dykes of magnetite as the source for all the groups. Though the amplitude of the airborne high associated with Group 1 is exceptionally large (more than two or three times that of the other group highs) it does not rule out a presence of smaller magnetite vein systems. This possibility was investigated by modelling one of the airborne profiles, that across Group 2, to determine the nature of bodies and their susceptibilities that could reproduce the central high.

Model for Group 2 airborne peak profile near past producer Crescent

A 2000 m long magnetic profile crossing the Group 2 peaks (*see* Fig. 5 for location) is displayed in Figure 12a, and the derived model is in Figure 12b. Approximately two-thirds of the southwest-northeast profile crosses the Pothook dioritic phase before traversing the monzonitic to monzodioritic Cherry Creek phase at the northeast end. A prominent high, amplitude roughly 4000 nT relative to the background magnetic field to the southwest, lies near the centre of the

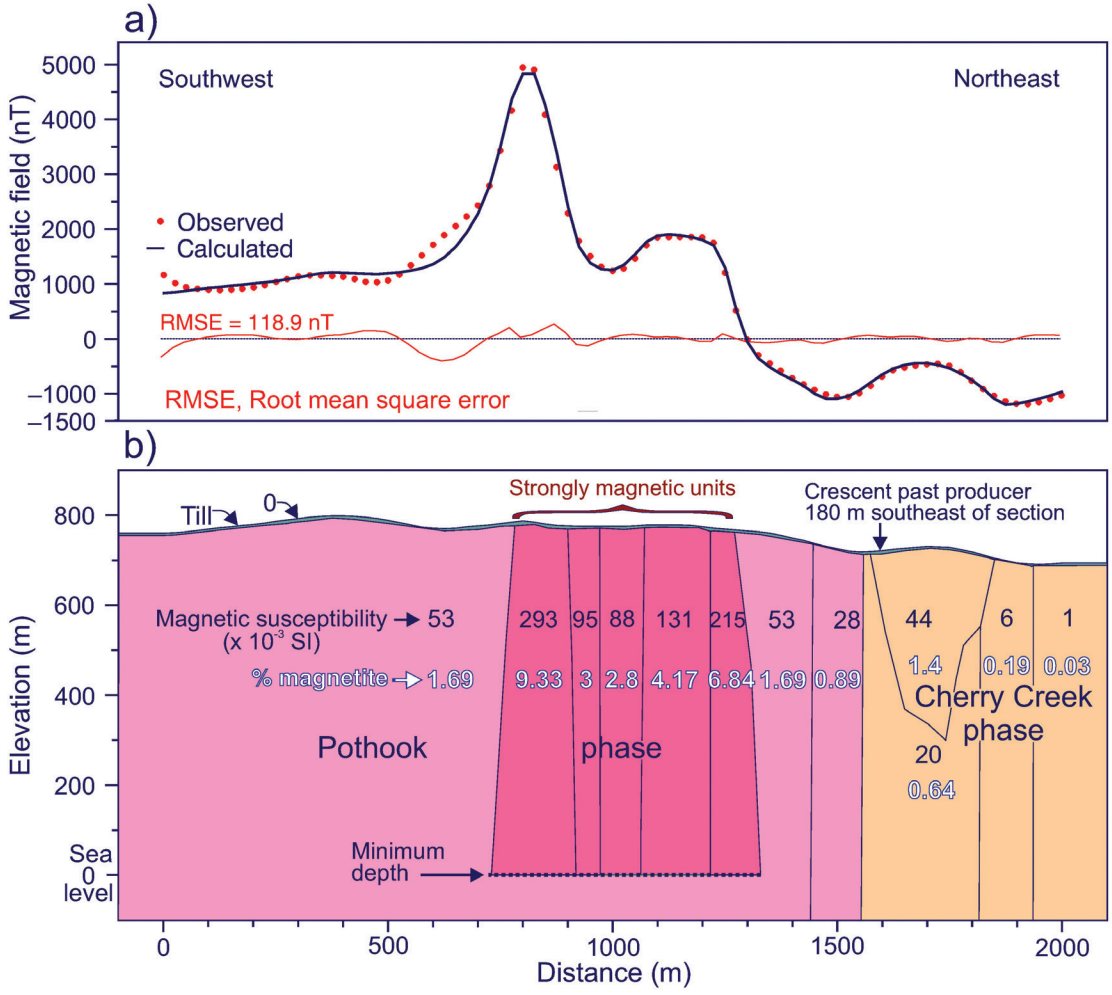

Figure 12: a) Modelled magnetic profile crossing peaks Group 2 (Fig. 5). **b)** Model derived from profile in a). The Pothook and Cherry Creek phases extend to a depth of 5000 m below sea level.

Pothook phase. It is flanked to the northeast, within the Pothook phase, by a conspicuous high with a much lower amplitude of almost 1000 nT relative to the same background. The magnetic field decreases significantly over the northeastern margin of the Pothook phase and the adjoining Cherry Creek phase, within which, with the exception of a broad low-amplitude high, it lies approximately 2000 nT lower than over the southwestern half of the Pothook phase.

The change in level is modelled essentially in terms of a large difference in the magnetic susceptibilities of the two plutonic phases. An arbitrary susceptibility of 20×10^{-3} SI and depth below surface of 5700 m was assigned to the Cherry Creek phase. The depth is similar to that modelled for a profile crossing the Iron Mask pluton farther to the southeast (Thomas, 2019). The base of the Pothook phase was set at the same level, and its susceptibility (53×10^{-3} SI) was determined during the modelling process, which sought as one objective to explain the generally higher magnetic field over this phase (Fig. 12b). The central magnetic high is explained by a narrow (average width $\approx$ 1700 m) vertical block with a strong magnetic susceptibility of 293×10^{-3} SI that descends from near surface to a depth of almost 780 m. An approximately 5 to 10 m thick surficial bed of non-magnetic overburden has been arbitrarily introduced into the model to simulate glacial till in the area. Several other vertical blocks are modelled within the Pothook phase to explain the magnetic high that is flanking the central magnetic high to the northeast, descending to the same depth as that explaining the central high. These have susceptibilities ranging from 88 to 215×10^{-3} SI. The modelled depth of the bottoms of these vertical blocks is considered the critical depth below which deepening of the blocks would not significantly change the magnetic response; hence, it is considered a minimum depth. During the modelling process, the original susceptibility of 20×10^{-3} SI assigned to the Cherry Creek phase was lowered to 6×10^{-3} and 1×10^{-3} SI in the northeastern margin of the phase.

Using the formula by McCafferty et al. (2004) the two largest susceptibilities, 215×10^{-3} SI and 293×10^{-3} SI, indicate magnetite contents of 6.8 and 9.3%, respectively, the latter being within the unit associated with the central magnetic high. These are much lower than the values ranging from 15.9 to 21.6% corresponding to the three highest susceptibilities modelled for the ground magnetic profile crossing Group 1. Nevertheless, they point to possible higher magnetite percentages within magnetic veins and/or dykes, as observed at the Magnet deposit. Considering the similarity in widths and amplitudes of principal magnetic highs along profiles crossing other peak groups (Fig. 8), concentrations of magnetic veins as a source of the observed magnetic highs are a reasonable geological explanation. If such dykes exist in proximal locations to Cu-Au mineral showings, what is their significance for mineral exploration?

SIGNIFICANCE OF MAGNETITE DYKES FOR CU-AU EXPLORATION

Despite the relatively intricate hydrothermal histories of mineral occurrences in the Iron Mask batholith, the association of magnetite with mineralization is spatially and apparently temporally close. Thus, magnetic surveys have a critical role in exploration of porphyry deposits. A challenge is how to derive the best information from the magnetic perspective.

A reasonably close spatial association between groups of strong magnetic peaks and mineral occurrences within the Iron Mask batholith has been noted (Fig. 4–7); however, with the exception of the Copper King (Cu, Au, Ag, U) and Magnet (mainly magnetite) past producers, the mineral occurrences are peripheral to the areas covered by the groups. The argument that they probably relate to concentrations of magnetite dykes has been presented. If this is true, what, if any, is the significance of these strong magnetic signatures for exploration of porphyry deposits?

Cann (1979) noted that magnetite-apatite lodes (dykes) in the batholith occur in close association with alkaline porphyry-type copper mineralization, disseminated magnetite-rich diorite, and late syenite, prompting a proposal that they could be used as a general exploration guide. Lode and disseminated magnetites were studied using atomic absorption spectrophotometry to examine several elements with a view to establishing a genetic model; several samples were also analyzed for minor and major oxides using an electron microprobe. Minor element data indicate that the lodes formed by magmatic injection subsequent to concentration of magnetite by immiscibility between magnetite-apatite and an alkalic magma. Cann (1979) proposed that the Pothook diorite developed by settling of plagioclase and pyroxene crystals within an early magma, leading to enrichment of iron and alkalis in a residual magma; the early magma also differentiated towards the experimentally determined magnetite-apatite eutectic composition. Following crystallization of the Pothook diorite, magnetite and apatite separated from the silicate magma, together forming an immiscible melt and settling on the floor of the magma chamber. This melt was subsequently injected into fractures, forming lodes after the adjacent younger Cherry Creek magma had largely crystallized (Cann, 1979).

Explosively emplaced breccia within the Cherry Creek phase and associated copper mineralization are attributed to a vapour bubble formed during the final stages of crystallization (Cann, 1979). Mineralization at the New Afton deposit is hosted in shattered rocks centred on such an intrusive breccia, and the deposit is contained within a 300 m wide zone of abundant magnetite that extends southeast to the Magnet mineral occurrence. Magnetite-apatite and copper mineralization at the New Afton deposit are believed to be genetically related, but not coeval, because copper mineralization and breccia emplacement are younger than the

magnetite-apatite lodes (Cann, 1979). The same magma phase was believed to be parent to both magnetite and copper mineralization.

Logan and Mihalynuk (2005) are in general agreement with Cann's (1979) temporal sequence of mineralization, noting that magnetite veins in the New Afton pit predate and accompany copper mineralization, and may be part of the same event that produced dilational veins at the Magnet mine; however, they do not favour magmatic injection as the process involved in creation of magnetite lodes, preferring a hydrothermal origin. Magnetite-apatite-actinolite-epidote veins at the New Afton pit and the Magnet occurrence are described as hydrothermal, and no significant amount of copper or gold was introduced during this early hydrothermal event. At the Pothook deposit, copper-gold mineralization postdates development of magnetite-apatite-actinolite veins (Stanley, 1994).

Based on these examples of mineral paragenesis in the Iron Mask batholith, it is reasonable to assume Cu-Au mineralization and magnetite-apatite mineralization may be linked to the same episode of magmatic-hydrothermal activity, with magnetite mineralization preceding Cu-Au mineralization. Richards et al. (2016) noted that Cu±Mo±Au (porphyry) and IOCG deposits share several key characteristics, particularly enrichments in Cu, Au, and Fe. The principal difference is in their respective predominant form of iron, with Fe sulfides predominating in porphyry deposits and Fe oxides (magnetite and hematite) in IOCG deposits. Because magnetite-apatite deposits are perhaps more commonly associated with IOCG deposits than with porphyry deposits, the relationship between magnetite-apatite dykes and Cu-Au mineralization associated with IOCG deposits may provide insight into the significance of magnetite-apatite dykes for exploration of porphyry Cu-Au deposits. Some examples of IOCG magnetite-apatite deposits (IOA) are now examined (Knipping et al., 2015a; Edfelt, 2007).

Some characteristics of magnetite-apatite mineralization associated with iron oxide-copper-gold deposits

Knipping et al. (2015a) investigated the formation and evolution of the Los Colorados IOA deposits in northern Chile through the geochemistry of magnetite with research that included targeting certain trace elements. Results are consistent with a magmatic-hydrothermal model for formation of IOA deposits proposed by Knipping et al. (2015b), involving crystallization of magnetite microlites from a silicate melt, nucleation of aqueous fluid bubbles on magnetite surfaces, and formation and ascent of buoyant fluid bubble-magnetite aggregates. The aggregates ascended through hydraulic fractures along the Atacama fault system, producing dyke-shaped Fe deposits. The magnetite dykes and an adjacent brecciated dioritic intrusion have similar radiometric ages, implying a possible genetic association. Magnetite from the diorite indicates lower temperature hydrothermal processes characteristic of IOCG deposits that are often observed in close relationship with IOA deposits. Knipping et al. (2015a) concluded that an IOCG deposit located laterally to, or stratigraphically above, an IOA system is a possibility, and that an underlying intrusion could provide sufficient Fe for both types of deposit.

In Sweden, Edfelt's (2007) study of the Tjårrojåkka apatite-iron and copper (-gold) deposits revealed similarities in stable isotope and fluid composition, temperature of ore deposition, and ages and assemblages of alterations and mineralization, indicating a genetic link between at least some of these deposit types. Mineralization is ascribed to two stages, with an earlier magnetite ore stage (I) and subsequent, overlapping, copper (chalcopyrite) ore stage (II); there are also two post-ore stages (III and IV). The δD_{H2O} values of fluids from the two deposits overlap, implying the same origin for the fluids involved in their formation. The trend of $\delta^{34}S$ values becomes increasingly larger from stage I to stage III of the paragenesis, suggesting that all mineralization was related to a single evolving system.

Arguments for a single system have been made also by Sillitoe (2003). He considered that the close association between magnetite-dominated IOCG and massive magnetite-(apatite) veins containing minor copper in several districts may signify that the two deposit types are transitional and that copper contents of IOCG veins may decrease downward with the development of massive magnetite veins. The district- and deposit-scale geological evidence, especially the intimate association between IOCG and massive magnetite deposits in parts of the Coastal Cordillera, does not support radically different fluid sources for the two deposit types.

The examples of Cu-Au and magnetite-apatite mineralization within the porphyry-type Iron Mask batholith and within areas of IOCG-type mineralization consistently suggest development of both types of mineralization being related to a single intrusive event, whether mineralization is magmatic, hydrothermal, or magmatic-hydrothermal. Depending on the many physical and chemical factors that influence development of a particular mineral(s) in intrusive systems, this provides encouragement that where one type of mineralization is present, the other type may also be present; however, a consistent pattern in the spatial distribution of the two types of mineralization is apparently not recognized, other than IOA deposits seemingly being generated at lower levels than IOCG deposits. Knipping et al. (2015a) pointed to experimental data supporting the scavenging of significant quantities of metals, for example, Cu and Au from a silicate melt by a saline magmatic-hydrothermal ore fluid. When combined with solubility data for Fe, Cu, and Au, it was considered reasonable that ore fluid continuing to rise from the IOA depositional environment can retain sufficient concentrations of these metals to form IOCG deposits at lateral and/or stratigraphically higher levels in the crust. As previously noted, Sillitoe (2003) also concluded that IOA

deposits developed at a lower crustal level than associated IOCG deposits. The scenarios of Knipping et al. (2015a) and Sillitoe (2003), if also applicable to porphyry deposits, are not entirely encouraging for exploration using magnetite-apatite mineralization as a guide because the presence of such mineralization near or at surface could mean that higher level Cu-Au mineralization has been eroded.

On a more positive note, Knipping et al. (2015a) concluded that an IOCG deposit located laterally to an IOA system is a possibility. In this regard, in the Iron Mask batholith, the New Afton deposit is located laterally to the Magnet magnetite-apatite deposit, near the end of the linear magnetic high passing through the Magnet deposit. Several other mineral occurrences in the Iron Mask batholith are also positioned laterally to groups of prominent magnetic highs (Fig. 5, 7). Modelling of a ground magnetic profile crossing Group 1 and of an airborne magnetic profile crossing Group 2 in the Iron Mask pluton presents reasonably strong evidence that the groups may relate to concentrations of magnetite veins or small dykes that could represent IOA-type mineralization. If this is the case, and the peak groups signal proximity to porphyry deposits, detailed multidisciplinary ground investigations are required in such presumed favourable areas. A method having good potential for such follow-up exploration is afforded by radiometric surveys, examined briefly below.

RADIOMETRIC SIGNATURES

The association of potassic alteration with some of the mineral occurrences in the Iron Mask pluton provides another avenue for exploration, namely via radiometric surveys that measure potassium (K), equivalent thorium (eTh), and equivalent uranium (eU). Shives et al. (1997) reported that many alkaline and calc-alkaline porphyry Au-Cu (±Mo) deposits are associated with extensive potassic hydrothermal alteration halos. Elevated potassium values do not necessarily signify related alteration but could relate to intrinsic lithological variations. This ambiguity can often be resolved by examining Th-K ratios because thorium is relatively stable during hydrothermal alteration and Th-K ratios are likely to decrease in localities subjected to potassic alteration (i.e. addition of potassium). Concentrations of low ratios (Th-K lows) could, therefore, correlate with areas of alteration and related mineralization. It is cautioned that radiometric signatures related to surficial glacial deposits may be displaced from any actual bedrock source for materials within the deposits producing the signatures. The map by Ferbey et al. (2013) shows ice-flow directions in the area of the batholith as being directed between approximately south-southeast and east-southeast.

Shives et al. (1995) reported on radiometric data measured at a mean terrain clearance of 120 m in a multiparameter survey (500 m line-spacing) of the batholith flown in 1993 (Shives and Carson, 1995). They noted that strong correlations between Th-K lows and flanking positive magnetic anomalies were associated with alteration related to mineralization in the areas of the New Afton, Ajax East, and Ajax West deposits, further stating that virtually every known deposit has this signature and that new targets were evident in several areas. The Kamloops survey provided slightly better resolution, having 400 m line-spacing, though flight elevation was practically the same (125 m).

A map of the Th-K ratio is shown in Figure 13. Distinct areas of low Th-K ratio are defined essentially by ratios less than the contour value of 2, displayed as dark blue areas, which cover approximately half of the Iron Mask pluton. The lows do not display any close correlation with the various phases of the pluton, falling equally within the intermediate Pothook, Sugarloaf, and Hybrid phases (typically dioritic) and the somewhat more acidic Cherry Creek phase (typically monzonitic), and frequently crossing contacts between phases at high angles. Remarkably, 40 of the 50 mineral occurrences displayed in this figure fall within, or are right at the edge of, these Th-K lows. Of the 16 past producers or developed prospects, only Iron Mask and Big Onion are not associated with a Th-K low. Although Shives et al. (1995) reported that alteration related to mineralization was associated with strong correlations between Th-K lows and flanking positive magnetic anomalies, it seems that, more specifically, the more intense magnetic highs are essentially co-located with Th-K lows. With the exception of Group 2, all groups of magnetic peaks in the Iron Mask pluton fall within Th-K lows.

A corridor of potassium alteration trending eastward from the New Afton deposit and encompassing the DM, Audra, Crescent, and Big Onion mineral occurrences (Logan and Mihalynuk, 2005) is partially reflected in the Th-K image as a distinct low trending northeast from the Pothook occurrence for approximately 3 km and ending at the Crescent occurrence. The low does not continue eastward to the Big Onion occurrence, approximately 2.5 km away, which falls on a Th-K high. A similar pattern is observed in an image of K values. Curiously, the New Afton deposit, reported to fall at the intersection of the K corridor with a northwest-trending corridor of albitic alteration (Logan and Mihalynuk, 2005), coincides with a local Th-K high (Fig. 13) and a K high. A belt of two Th-K lows extending southeast from the vicinity of the Rainbow developed prospect encompasses three nearby showings west-northwest of Wallender Lake and continues to Jacko Lake, where it swings east to include the Ajax West and Ajax East past producers. From Ajax East the belt broadens significantly as it extends both east-northeast and north-northeast to occupy much of the marginal area of the Iron Mask pluton along its eastern boundary. Notable mineral occurrences within this area of Th-K lows are the Python past producer and Kimberley developed prospect.

The pattern of Th-K variations is noticeably similar to the pattern over the mainly mafic Nicola Group volcanic rocks southwest of the Iron Mask pluton; however, because of the volcanic nature of the terrain in this area, the

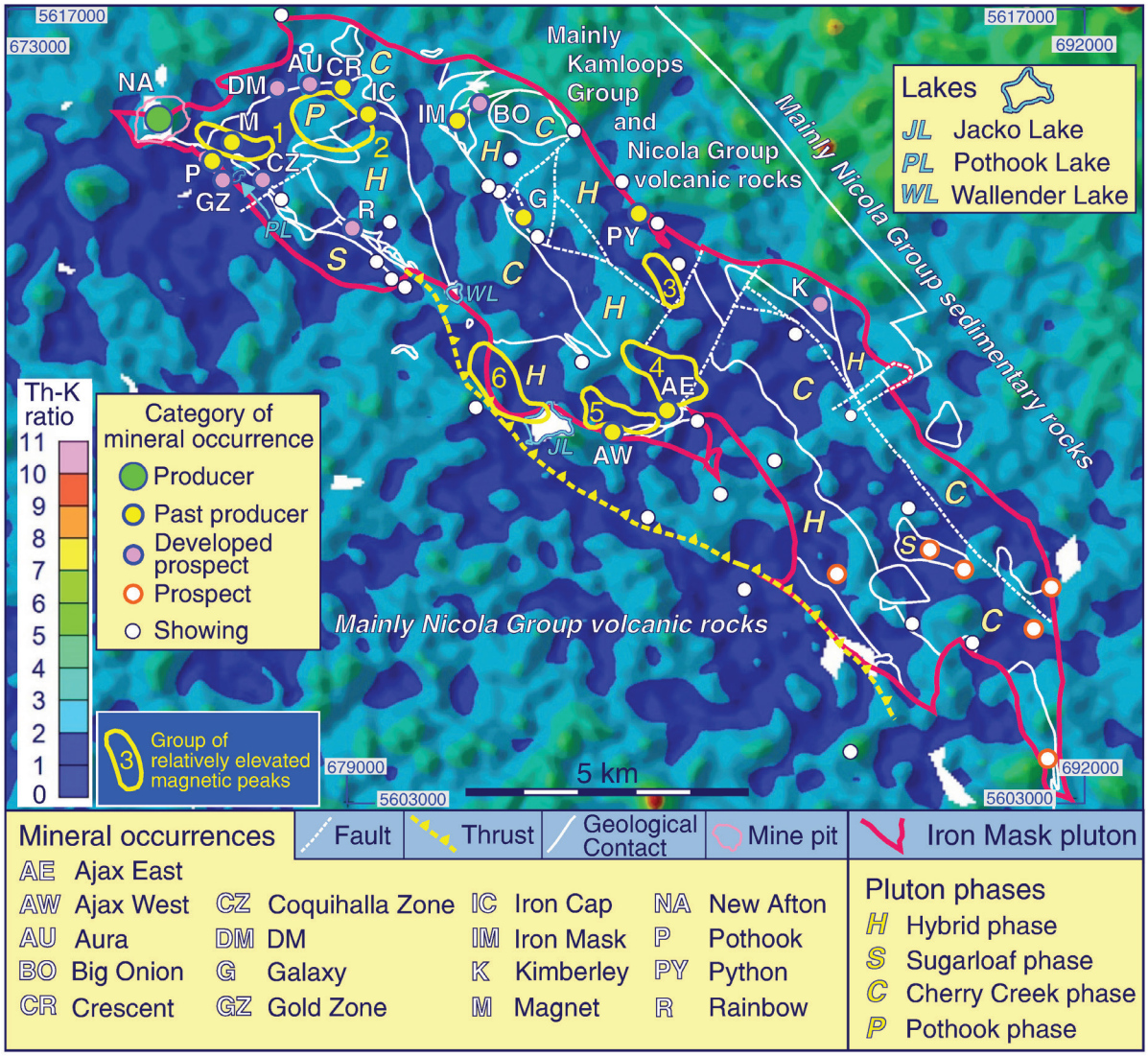

Figure 13: Map of Th-K ratio for the Iron Mask pluton displaying locations of mineral occurrences, areas of relatively elevated magnetic peak values, geological contacts and faults within the pluton; phases of the pluton are identified

significance of the Th-K lows is probably different from that of the lows within the pluton. Killeen's (1979) table of values for radio-element concentrations in different rock type categories indicates that intermediate intrusive rocks have noticeably higher values of K (2.1%) and Th (12.2 ppm), than intermediate extrusive rocks, which have 1.1% and 2.4 ppm, respectively; hence, even without the addition of hydrothermal potassium, the extrusive varieties would theoretically produce a lower Th-K ratio (2.18) than their intrusive counterparts (5.81). The Th-K ratio for basic extrusive rocks (K 0.7%, Th 2.2 ppm) is 3.14. It is difficult, therefore, to attach significance to the patterns of Th-K ratio over the Nicola Group intermediate-basic volcanic rocks, other than to conjecture that they reflect heterogeneity within the volcanic sequences and perhaps a variable presence of sedimentary rocks.

The production of potassium and magnetite related to hydrothermal alteration associated with porphyry-related mineralization, and the described spatial relationships of peak magnetic highs, potassium, and Th-K ratios within the Iron Mask batholith make a compelling case for the inclusion of magnetic and radiometric surveys in exploration strategies for porphyry deposits.

DISCUSSION AND CONCLUSIONS

Despite the relatively intricate hydrothermal histories of mineral occurrences in the Iron Mask batholith, the association of magnetite with porphyry-type mineralization is spatially and possibly temporally close. Lang (1994), for example, noted early K metasomatism at the Crescent

deposit being "closely followed in sequence" by a variety of vein types including magnetite and Cu ore-bearing chlorite-sulfide veins. Magnetic surveys have a critical role in exploration of porphyry deposits, a strategy seemingly founded on Sillitoe's (1979) observation of the common association of significant quantities of magnetite with potassium silicate alteration in gold-rich porphyry copper deposits. More specifically, Sillitoe (1979) suggested that airborne magnetic surveys could be effective in locating deposits, and that if the gold-bearing character of a prospect could be established, drilling could be focused in the vicinity of the highest magnetic response. This strategy may apply to instances of 'well-behaved' porphyry mineralization within stock-like intrusions having symmetrical, concentric alteration-mineralization zones as envisaged in the ovoid porphyry model of Lowell and Guilbert (1970); however, in reality, porphyritic intrusions do not always conform to this type model and may be complex in terms of structure, composition, and the number of phases of intrusion and hydrothermal activity, all of which, individually or in concert, can disrupt initially simple mineralogical or geochemical patterns. The Iron Mask pluton does not conform to the typical concentric model of Lowell and Guilbert (1970), but rather is an elongate intrusion composed in large part of subparallel, belt-like intrusive phases. Despite this difference, magnetite in significant quantities is present.

Notwithstanding potential complications related to nonconformity of an intrusion with a type intrusion, the documented association of magnetite and gold-rich porphyry copper deposits, and of magnetite-apatite deposits (IOA) with porphyry and IOCG deposits, dictates that targeting magnetite via distinct magnetic anomalies in the search for porphyry deposits is a critical element in exploration. The study of relationships between prominent magnetic highs and porphyry Cu-Au mineral occurrences in the alkalic Iron Mask batholith supports this approach. A substantial number of occurrences are positioned peripherally to clusters of prominent magnetic peaks with the nearest located an average of approximately 500 m from the centre of a cluster. These spatial relationships are encouraging from the viewpoint of magnetic exploration, dramatically reducing the size of an area for follow-up exploration.

The alkalic Iron Mask batholith is radically different from the concentric, alteration-mineralization, stock-like porphyry intrusion model of Lowell and Guilbert (1970). It is an elongate intrusion with a length-to-width ratio of approximately 7:1, is composed mainly of dioritic rocks rather than the typical quartz monzonite of the model, and more than 50 mineral occurrences are scattered throughout, in contrast to the apparently singular orebodies associated with the Lowell and Guilbert (1970) model. The common trait of both types of Cu-Au host is the close spatial and genetic association of Cu-Au mineralization with magnetite (plus apatite) mineralization. Thus, magnetic surveys offer a critical approach in exploration strategies directed toward the discovery of porphyry-type deposits, regardless of the nature of the hosting intrusion. The presence of hydrothermal potassium in alteration zones associated with such deposits provides another avenue for exploration through delineation of Th-K lows, yielding information complementing the magnetic signatures. Both types of data can be rapidly collected in a single combined magnetic-radiometric airborne survey.

ACKNOWLEDGMENTS

I thank my colleague, Ernst Schetselaar, for his insightful review of the manuscript, and related comments and suggestions. I also thank Devin Wade at New Gold Inc., Kamloops, British Columbia, for providing information on rock properties and a high-resolution magnetic data set covering much of the Iron Mask batholith, and ground gravity and magnetic data near the New Afton pit. My thanks to Chris Ludwig, consulting geophysicist, Denver, Colorado, consultant to New Gold Inc., for his insight into interpretation of the ground data sets.

REFERENCES

Arancibia, O.N. and Clark, A.H., 1996. Early magnetite-amphibole-plagioclase alteration-mineralization in the Island Copper porphyry copper-gold-molybdenum deposit, British Columbia; Economic Geology, v. 91, no. 2, p. 402–438. https://doi.org/10.2113/gsecongeo.91.2.402

Balsley, J.R. and Buddington, A.F., 1958. Iron-titanium oxide minerals, rocks, and aeromagnetic anomalies of the Adirondack area, New York; Economic Geology, v. 53, no. 7, p. 777–805. https://doi.org/10.2113/gsecongeo.53.7.777

British Columbia Geological Survey, 2018a. MapPlace GIS internet mapping system; British Columbia Ministry of Energy, Mines and Petroleum Resources, British Columbia Geological Survey. <http://www.MapPlace.ca> [accessed February 14, 2019]

British Columbia Geological Survey, 2018b. Mineral inventory; British Columbia Ministry of Energy, Mines and Petroleum Resources, British Columbia Geological Survey. <https://www2.gov.bc.ca/gov/content/industry/mineral-exploration-mining/british-columbia-geological-survey/mineralinventory> [accessed February 14, 2019]

British Columbia Geological Survey, 2018c. MINFILE 092INE010 record summary, MINFILE BC mineral deposits database; British Columbia Ministry of Energy, Mines and Petroleum Resources, British Columbia Geological Survey. <https://minfile.gov.bc.ca/Summary.aspx?minfilno=092INE010> [accessed February13, 2020]

British Columbia Geological Survey, 2018d. MINFILE 092INE002 record summary, MINFILE BC mineral deposits database; British Columbia Ministry of Energy, Mines and Petroleum Resources, British Columbia Geological Survey. <https://minfile.gov.bc.ca/Summary.aspx?minfilno=092INE002> [accessed February 14, 2020]

British Columbia Geological Survey, 2018e. MINFILE 092INE013 record summary, MINFILE BC mineral deposits database; British Columbia Ministry of Energy, Mines and Petroleum Resources, British Columbia Geological Survey. <https://minfile.gov.bc.ca/Summary.aspx?minfilno=092INE013> [accessed February 14, 2020]

British Columbia Geological Survey, 2018f. MINFILE 092INE023 record summary, MINFILE BC mineral deposits database, British Columbia Ministry of Energy, Mines, and Petroleum Resources, British Columbia Geological Survey. <https://minfile.gov.bc.ca/Summary.aspx?minfilno=092INE023> [accessed February 13, 2020]

British Columbia Geological Survey, 2018g. MINFILE 092INE098 record summary, MINFILE BC mineral deposits database; British Columbia Ministry of Energy, Mines and Petroleum Resources, British Columbia Geological Survey. <https://minfile.gov.bc.ca/Summary.aspx?minfilno=092INE098> [accessed February 15, 2020]

British Columbia Geological Survey, 2018h. MINFILE 092INE025 record summary, MINFILE BC mineral deposits database; British Columbia Ministry of Energy, Mines and Petroleum Resources, British Columbia Geological Survey. <https://minfile.gov.bc.ca/Summary.aspx?minfilno=092INE025> [accessed February 15, 2020]

British Columbia Geological Survey, 2018i. MINFILE 092INE024 record summary, MINFILE BC mineral deposits database; British Columbia Ministry of Energy, Mines and Petroleum Resources, British Columbia Geological Survey. <https://minfile.gov.bc.ca/Summary.aspx?minfilno=092INE024> [accessed February 15, 2020]

British Columbia Geological Survey, 2018j. MINFILE 092INE031 record summary, MINFILE BC mineral deposits database; British Columbia Ministry of Energy, Mines and Petroleum Resources, British Columbia Geological Survey. <https://minfile.gov.bc.ca/Summary.aspx?minfilno=092INE031> [accessed February 15, 2020]

British Columbia Geological Survey, 2018k. MINFILE 092INE055 record summary, MINFILE BC mineral deposits database; British Columbia Ministry of Energy, Mines and Petroleum Resources, British Columbia Geological Survey. <https://minfile.gov.bc.ca/Summary.aspx?minfilno=092INE055> [accessed February 15, 2020]

British Columbia Geological Survey, 2018l. MINFILE 092INE032 record summary, MINFILE BC mineral deposits database; British Columbia Ministry of Energy, Mines and Petroleum Resources, British Columbia Geological Survey. <https://minfile.gov.bc.ca/Summary.aspx?minfilno=092INE032> [accessed February 15, 2020]

British Columbia Geological Survey, 2018m. MINFILE 092INE029 record summary, MINFILE BC mineral deposits database; British Columbia Ministry of Energy, Mines and Petroleum Resources, British Columbia Geological Survey. <https://minfile.gov.bc.ca/Summary.aspx?minfilno=092INE029> [accessed February 15, 2020]

British Columbia Geological Survey, 2018n. MINFILE 092INE022 record summary, MINFILE BC mineral deposits database; British Columbia Ministry of Energy, Mines and Petroleum Resources, British Columbia Geological Survey. <https://minfile.gov.bc.ca/Summary.aspx?minfilno=092INE022> [accessed February 15, 2020]

Cann, R.M., 1979. Geochemistry of magnetite and the genesis of magnetite-apatite lodes in the Iron Mask batholith, British Columbia; M.Sc. thesis, The University of British Columbia, Vancouver, British Columbia.

Carr, J.M. and Reed, A.J., 1976. Afton: A supergene copper deposit; *in* Porphyry deposits of the Canadian Cordillera, (ed.) A. Sutherland Brown; Canadian Institute of Mining and Metallurgy, Special Volume 15, p. 376–387.

Clark, D.A., 2014. Magnetic effects of hydrothermal alteration in porphyry copper and iron-oxide copper–gold systems: A review; Tectonophysics, v. 624–625, p. 46–65. https://doi.org/10.1016/j.tecto.2013.12.011

Edfelt, Å., 2007. The Tjårrojåkka apatite-iron and Cu (-Au) deposits, northern Sweden. Ph.D. thesis, Luleå University of Technology, Luleå, Sweden.

Ferbey, T., Arnold, H., and Hickin, A.S., 2013. Ice-flow indicator compilation, British Columbia; British Columbia Geological Survey, Open File 2013-06, Sheet 1 of 2, scale 1:1 650 000.

Killeen, P.G., 1979. Gamma ray spectrometric methods in uranium exploration – application and interpretation; *in* Geophysics and geochemistry in the search for metallic ores, Proceedings of Exploration 77; Geological Survey of Canada, Economic Geology Report 31, p. 163–229. https://doi.org/10.4095/106049

Knipping, J.L., Bilenker, L.D., Simon, A.C., Reich, M., Barra, F., Deditius, A.P., Wälle, M., Heinrich, C.A., Holtz, F., and Munizaga, R., 2015a. Trace elements in magnetite from massive iron oxide-apatite deposits indicate a combined formation by igneous and magmatic-hydrothermal processes; Geochimica et Cosmochimica Acta, v. 171, p. 15–38. https://doi.org/10.1016/j.gca.2015.08.010

Knipping, J.L., Bilenker, L.D., Simon, A.C., Reich, M., Barra, F., Deditius, A.P., Lundstrom, C., Bindeman, I., and Munizaga, R., 2015b. Giant Kiruna-type deposits form by efficient flotation of magmatic magnetite suspensions; Geology, v. 43, no. 7, p. 591–594, https://doi.org/10.1130/G36650.1

Kwong, Y.T.J., 1987. Evolution of the Iron Mask batholith and its associated copper mineralization; British Columbia Ministry of Energy, Mines and Petroleum Resources, Mineral Resources Division, British Columbia Geological Survey, Bulletin 77, 55 p., 1 map, scale 1:50 000.

Lang, J.R., 1994. Geology of the Crescent alkalic porphyry copper-gold deposit, Afton mining camp, British Columbia (92I/9); *in* Geological Fieldwork 1993, a summary of field activities and current research, (ed.) B. Grant and J.M. Newell; British Columbia Ministry of Energy, Mines and Petroleum Resources, British Columbia Geological Survey, Paper 1994-1, p. 285–296.

Lang, J.R. and Stanley, C.R., 1995. Contrasting styles of alkalic porphyry copper-gold deposits in the northern part of the Iron Mask batholith, Kamloops, British Columbia; *in* Porphyry deposits of the northwestern Cordillera of North America, (ed.) T.G. Schroeter; Canadian Institute of Mining, Metallurgy and Petroleum, Special Volume 46, p. 581–592.

Logan, J.M. and Mihalynuk, M.G., 2005. Porphyry Cu-Au deposits of the Iron Mask batholith, southeastern British Columbia; *in* Geological Fieldwork 2004, British Columbia Ministry of Energy, Mines and Petroleum Resources, British Columbia Geological Survey, Paper 2005-1, p. 271–290.

Logan, J.M., Mihalynuk, M.G., Ullrich, T.D., and Friedman, R., 2006. Geology of the Iron Mask batholith; British Columbia Ministry of Energy, Mines and Petroleum Resources, British Columbia Geological Survey, Open File Map 2006-11, scale 1:25 000.

Lowell, J.D. and Guilbert, J.M., 1970. Lateral and vertical alteration-mineralization zoning in porphyry ore deposits; Economic Geology, v. 65, no. 4, p. 373–408. https://doi.org/10.2113/gsecongeo.65.4.373

McCafferty, A.E., Van Gosen, B.S., Smith, B.D., and Sole, T.C., 2004. Geophysical characterization of geologic features with environmental implications from airborne magnetic and apparent resistivity data; Chapter D2 of Integrated investigations of environmental effects of historical mining in the Basin and Boulder mining districts, Boulder River Watershed, Jefferson County, Montana, (ed.) D.A. Nimick, S.E. Church, and S.E. Finger; U.S. Geological Survey, Professional Paper 1652-D2, p. 90–125.

Mortensen, J.K., Ghosh, D.K., and Ferri, F., 1995. U-Pb geochronology of intrusive rocks associated with copper-gold porphyry deposits in the Canadian Cordillera; *in* Porphyry deposits of the northwestern Cordillera of North America, (ed.) T.G. Schroeter; Canadian Institute of Mining, Metallurgy and Petroleum, Special Volume 46, p. 142–158.

Richards, J.P., López, G.P., Zhu, J.-j., and Mumin, A.H., 2016. Links between porphyry and IOCG deposits, Paper 5292, Session T18.1, Ore-forming processes associated with hypabyssal magmatic and related volcanic systems; 35th International Geological Congress, 22nd August – 2nd September 2016, Cape Town, South Africa (abstract). https://www.americangeosciences.org/information/igc/

Ross, K.V., Godwin, C.I., Bond, L., and Dawson, K.M., 1995. Geology, alteration and mineralization of the Ajax East and Ajax West copper-gold alkali porphyry deposits, southern Iron Mask batholith, Kamloops, British Columbia; *in* Porphyry deposits of the northwestern Cordillera of North America, (ed.) T.G. Schroeter, Canadian Institute of Mining, Metallurgy and Petroleum, Special Volume 46, p. 565–580.

Schetselaar, E.M., Bellefleur, G., Craven, J.A., White, D., Thomas, M.D., Tschirhart, V.L., Pilkington, M., Enkin, R.J., Percival, J.A., and Percival, J.B., 2017. Integrated 3D model of magmatic-hydrothermal evolution of the Iron Mask batholith complex near the New Afton Mine; in Targeted Geoscience Initiative: 2016 report of activities, (ed.) N. Rogers; Geological Survey of Canada, Open File 8199, p. 69–73. https//doi.org/10.4095/299573

Shives, R.B.K. and Carson, J.M., 1995. Airborne geophysical survey, Ironmask batholith, British Columbia, NTS 92I/8, 9, 10, 15; Geological Survey of Canada, Open File 2817, 63 p., scale 1:150 000. https://doi.org/10.4095/203472

Shives, R.B.K., Ford, K.L., and Charbonneau, B.W., 1995. Geological Survey of Canada workshop manual: applications of gamma ray spectrometric/magnetic/VLF-EM surveys; Geological Survey of Canada, Open File 3061, 85 p. https://doi.org/10.4095/203485

Shives, R.B.K., Charbonneau, B.W., and Ford, K.L., 1997. The detection of potassic alteration by gamma-ray spectrometry - recognition of alteration related to mineralization; *in* Geophysics and geochemistry at the millenium: proceedings of Exploration 97, the fourth decennial international conference on mineral exploration, (ed.) A.G. Gubins; Prospectors and Developers Association of Canada, Toronto, Ontario, p. 741–752.

Sillitoe, R.H., 1979. Some thoughts on gold-rich porphyry copper deposits; Mineralium Deposita, v. 14, no. 2, p. 161–174. https://doi.org/10.1007/BF00202933

Sillitoe R.H., 2003. Iron oxide–copper–gold deposits: an Andean view; Mineralium Deposita, v. 38, no. 7, p. 787–812. https://doi.org/10.1007/s00126-003-0379-7

Snyder, L.D., 1994. Petrological studies within the Iron Mask batholith, south central British Columbia; M.Sc. thesis, The University of British Columbia, Vancouver, British Columbia, 192 p.

Snyder, L.D. and Russell, J.K., 1993. Field constraints on diverse igneous processes in the Iron Mask Batholith (92I9/10); *in* Geological Fieldwork 1992, (ed.) B. Grant and J.M. Newell; British Columbia Ministry of Energy, Mines and Petroleum Resources, British Columbia Geological Survey, Paper 1993-1, p. 281–286.

Snyder, L.D. and Russell, J.K., 1995. Petrogenetic relationships and assimilation processes in the alkali Iron Mask batholith, south-central British Columbia; *in* Porphyry deposits of the northwestern Cordillera of North America, (ed.) T.G. Schroeter; Canadian Institute of Mining, Metallurgy and Petroleum, Special Volume 46, p. 593–608.

Stanley, C.R., 1994. Geology of the Pothook alkalic copper-gold porphyry deposit, Afton Mining Camp, British Columbia (92I/9,10); *in* Geological Fieldwork 1993, (ed.) B. Grant and J.M. Newell; British Columbia Ministry of Energy, Mines and Petroleum Resources, British Columbia Geological Survey, Paper 1994-1, p. 275–284.

Stanley, C.R., Lang, J.R., and Snyder, L.D., 1994. Geology and mineralization in the northern part of the Iron Mask batholith, Kamloops, British Columbia (92I/9, 10); *in* Geological Fieldwork 1993, (ed.) B. Grant and J.M. Newell; British Columbia Ministry of Energy, Mines and Petroleum Resources, British Columbia Geological Survey, Paper 1994-1, p. 269–274.

Thomas, M.D., 2010. Geological significance of new aeromagnetic data from the Kamloops survey area (Portions of NTS 92I (Ashcroft) and 82L (Vernon)), central British Columbia: a Mountain Pine Beetle Program contribution; Geological Survey of Canada, Open File 6659, 55 p. https://doi.org/10.4095/286265

Thomas, M.D., 2019. Gravity and magnetic models of the Iron Mask batholith, south-central Canadian Cordillera, British Columbia; Geological Survey of Canada, Current Research 2019-1, 24 p. https://doi.org/10.4095/314517

Young, G.A. and Uglow, W.L., 1926. The iron ores of Canada, volume 1, British Columbia and Yukon; Geological Survey, Canada Department of Mines, Ottawa, Economic Geology Series 3, 253 p. https://doi.org/10.4095/103992